Title

Investigating the Role of Transcription Factor ZFHX4 in Human Corticogenesis

Author

Hebner, Yuki

Publication Date

2024

Peer reviewed|Thesis/dissertation

UNIVERSITY OF CALIFORNIA

Los Angeles

Investigating the Role of Transcription Factor ZFHX4 in Human Corticogenesis

A dissertation submitted in partial satisfaction of the requirements

for the degree Doctor of Philosophy in Molecular Biology

by

Yuki Christina Hebner

2024

ABSTRACT OF THE DISSERTATION

Investigating the Role of Transcription Factor ZFHX4 in Human Corticogenesis

by

Yuki Christina Hebner

Doctor of Philosophy in Molecular Biology

University of California, Los Angeles, 2024

Professor Luis de la Torre-Ubieta, Chair

The human neocortex arises from the carefully orchestrated production and maturation of neurons and glia from neural progenitor pools during development. The molecular mechanisms underlying human corticogenesis are not well understood, but critically important to understanding our complex cognitive abilities and how the dysregulation of these mechanisms can lead to intellectual impairment and neuropsychiatric disease. The activity of *cis* gene-regulatory elements (GREs) and their corresponding transcription factors (TFs) play a pivotal role in modulating cell-specific transcriptional programs that drive corticogenesis.

The emergence of genomic tools to profile gene expression and chromatin dynamics in single cells has facilitated the study of the interplay between gene regulatory elements and the TFs acting on these sites. Previously, our laboratory profiled transcriptional programs across developing neocortical cell types and identified several TFs enriched in neural progenitor cells located in the germinal zone (GZ) of the neocortex. In parallel, we profiled and contrasted

chromatin dynamics between the GZ and the neuron-enriched cortical plate (CP), identifying GREs predicted to drive gene expression programs during neurogenesis.

From these studies we identified a TF, ZFHX4, which is highly enriched in ventricular radial glia, and is the target of several GREs with enriched activity in the GZ. ZFHX4 has been implicated in several neurodevelopmental and intellectual disorders, including congenital bilateral isolated ptosis, syndromic Peters anomaly, and childhood apraxia of speech and has been reported to regulate cell differentiation at least in part through interactions with the chromatin remodeling complex NuRD.

Despite its clinical relevance and enriched expression within neural progenitors of the developing brain, the role of ZFHX4 in neocortical development has never been studied. I hypothesize that ZFHX4 coordinates human cortical neurogenesis through the NuRD chromatin remodeling complex by modulating radial glia cell proliferation and differentiation, and that ZFHX4 loss-of-function-related dysregulation of corticogenesis underlies neurological disorders.

Here, I detail the design, rationale, and outcomes of my efforts to identify the functional role and gene regulatory mechanisms of ZFHX4 in human neurogenesis using physiologically relevant neural stem cell models. In addition to characterizing a novel transcription factor, I have demonstrated the validity of using CRISPR-interference (CRISPRi) to functionally interrogate developmentally dynamic transcription factors like ZFHX4 and its putative GREs. Conducting CRISPRi experiments in complementary models of human corticogenesis have also contributed to developing an *in vivo* pipeline to study gene-regulatory functions and assess its role in lineage specification during cortical development. Altogether, these studies are expected to provide novel insights into mechanisms of human neocortical expansion and how their dysregulation leads to neurodevelopmental disorders.

The dissertation of Yuki Christina Hebner is approved.

Michael F. Carey

April D. Pyle

Thomas M. Vondriska

James A. Wohlschlegel

Luis de la Torre-Ubieta, Committee Chair

University of California, Los Angeles

2024

To my parents, Kevin and Yuiko

My siblings, Jacqui and Hiroshi

My grandparents, Marven, Joan and Helen

My dear friends, Kathryn, Alexandra, Sylwia, Virginia, Althea, Zoe, Justin and Sean

My pets, Sailor, Scott, Lucille and Hank

Table of Contents

Figure Index

Table Index

Acknowledgements

I would like to thank lab members who participated in key parts of this project. Dr. Luis de la Torre-Ubieta, alongside scientists in the lab of Dr. Geschwind, generated the genomic data leveraged for this project. Dr. Celine Vuong and Dr. Susanne Nichterwitz helped establish the organotypic slice culture (OSC) protocol, Dr. Vuong and Beck Schafie helped clone sgRNAs into a CRISPRi (ZIM3) plasmid, Dr. Vuong generated 10x libraries and assisted with Western blots, Valerie Doan quantified live images of the OSCs, and Alvin Tran helped develop the analysis pipeline. I especially thank Beck, Susanne and Allie Weber for their comradery over the last five years. I would like to acknowledge my funding sources and equipment facilities, including my Ruth L. Kirschstein National Research Service Award, Dr. de la Torre-Ubieta's funding from NIMH, the Broad Center of Regenerative Medicine and Stem Cell Research, the Intellectual and Developmental Disabilities Research Center Structural and Functional Visualization core, and the UCLA CFAR from which we collected human developing tissue.

Thank you to my committee members Dr. Carey, Dr. Vondriska, Dr. Pyle, and Dr. Wohlschlegel for four years of insight, support, and guidance. I would like to extend a special thank you to Dr. Carey, the former director of the Gene Regulation home area, who was instrumental to my training and perseverance in the MBIDP. I would also like to collectively thank the MBIDP home area directors for creating a learning environment that has been as warm and supportive as it has been exciting and challenging. Thank you, Dr. Felix Schweizer and the Brain Research Institute at UCLA, for supporting the creation of the Neuroscience Communication Affinity Group. Lastly, I would like to thank the awe-inspiring Dr. Julianne McCall, whose earnest, generous mentorship is unparalleled, as is her contribution to and influence in the field of precision medicine policy.

Vita

EDUCATION

PhD candidate, Molecular Biology Interdepartmental Program *October 2018 – June 2024*
University of California, Los Angeles. Los Angeles, CA
GPA: 3.68

Master of Arts, Molecular Biology & Biochemistry *June 2017 – May 2018*
Wesleyan University. Middletown, CT
GPA: 3.31

Bachelor of Arts, Molecular Biology & Biochemistry *September 2013 – May 2017*
Wesleyan University. Middletown, CT
GPA: 3.13

ACADEMIC RESEARCH & TEACHING

Graduate Student Researcher *April 2019 – May 2024*
Dr. Luis de la Torre-Ubieta, UCLA
Dissertation: Investigating the role of transcription factor ZFHX4 in human corticogenesis

Teaching Assistantship, Developmental Biology *January – March 2021*
Molecular, Cellular, and Integrative Physiology, UCLA *April – June 2020*

Director, Neuroscience Communication Affinity Group *September 2020 – 2022*
Brain Research Institute, UCLA

Graduate Student Researcher *June 2017 – May 2018*
Dr. Scott Holmes, Wesleyan University
Thesis: Linker, variant, & core histones: A collective effort to maintain genomic integrity

Work Study, Undergraduate Researcher *September 2015 – May 2017*
Dr. Scott Holmes, Wesleyan University

FELLOWSHIPS AND AWARDS

Science & Technology Policy Fellowship *September 2022 – current*
California Initiative to Advance Precision Medicine
The Governor of California's Office of Research & Planning

Ruth L. Kirschstein National Research Service Award *July 2019 – June 2021*
National Institutes of Health

Outstanding Original Research Presentation *December 2022*
Cedars Sinai Graduate Student Symposium

Fred Eiserling & Judith Lengyel Award for Teaching Excellence *October 2021*
Molecular Biology Interdepartmental Program, UCLA

SERVICE & LEADERSHIP

Editor, Knowing Neurons *November 2020 – 2022*
President, Science Policy Group at UCLA *September 2019 – 2022*
Volunteer Scientist, Skype a Scientist *October 2019 – 2022*
Leadership Team, AWiSE at UCLA *October 2019 – 20*

Chapter 1: Introduction

1.1 Human neocortical development

1.1.1 Evolution and development of the human neocortex

The neocortex is responsible for many higher-order cognitive and social capabilities such as sensory and emotional processing (de la Torre-Ubieta et al., 2016; Gandal et al., 2016; Krasnegor et al., 1997). Comparative cross-species studies indicate that the human cerebral cortex displays greater structural complexity and cellular heterogeneity than that of other mammalian species (Bae et al., 2015; Bystron et al., 2008; Lui et al., 2011; Sun & Hevner, 2014; Taverna et al., 2014) and that this is a central mechanism in the evolution of human cognition (Kang et al., 2011; Lodato & Arlotta, 2015; Miller et al., 2014; Nord et al., 2015; Nord & West, 2020).

The highly structured mammalian cerebral cortical wall is divided into laminae enriched for distinct cell types and functions. These layers are established by the spatial-temporal progression of neural progenitor cells (NPCs) in the germinal zone (GZ) into the cortical plate (CP) to become mature, specialized neurons. This process, called neurogenesis, is coordinated by precise gene regulatory programs that drive changes in cell composition through tightly regulated control of the proliferation, differentiation, and migration of neural progenitors (Kang et al., 2011; Lodato & Arlotta, 2015; Miller et al., 2014; Nord et al., 2015; Nord & West, 2020).

1.1.2 Cortical dysregulation: Intellectual disabilities and psychiatric disorders

While the evolutionary divergence of human corticogenesis contributes to our specialized cognitive abilities, the prolonged development and complexity confers both vulnerability and sensitivity to dysregulation (Geschwind & Rakic, 2013). Somatic mutations, epigenetic alterations, and environmental insults during brain development can impede our ability to

process higher-order information, regulate emotion, and perform complex behaviors, which may lead to neuropsychiatric and intellectual disorders. Consistently, genes causing or conferring risk for neuropsychiatric disorders are frequently expressed in the developing human neocortex and their perturbation in experimental models leads to cellular and behavioral phenotypes observed in these disorders (de la Torre-Ubieta et al., 2016). These alterations to normal corticogenesis, which include changes in cortical thickness, surface area, lamination and/or cell type identity, are caused by dysregulation in the differentiation and maturation of neural progenitors into the appropriate proportions and subtypes of mature neurons (Bae et al., 2015; de la Torre-Ubieta et al., 2016; Lui et al., 2011; Sun & Hevner, 2014).

1.1.3 The neocortical gene regulatory landscape

Significant advances have been made profiling transcriptomic diversity of cell types in the developing human brain (Kang et al., 2011; Lodato & Arlotta, 2015; Miller et al., 2014; Pollen et al., 2015; Xu et al., 2014; Braun et al., 2023; Polioudakis et al., 2019; Siletti et al., 2023; Velmeshev et al., 2023; Ziffra et al., 2021) yet the gene-regulatory mechanisms driving gene expression programs remain to be revealed. There is accumulating evidence that chromatin remodeling is a critical component of proper cognitive development (Day & Sweatt, 2011; Jakovcevski & Akbarian, 2012; Mehler, 2008; van Bokhoven, 2011; Won et al., 2016), and mutations in several chromatin remodelers have been associated with various neurodevelopmental and psychiatric disorders (Shain & Pollack, 2013; Wilson, 2008).

The activity of *cis* gene-regulatory elements (GREs) and their corresponding transcription factors (TFs) play a pivotal role in modulating cell-specific transcriptional programs that drive corticogenesis. Changes in chromatin conformation bring distal enhancers into physical

proximity with their corresponding promoters, and these GREs provide binding sites for TFs (Amano et al., 2009; Nord & West, 2020). In the developing neocortex, distinct TFs direct cellular proliferation, differentiation and cell fate/identity through incompletely understood mechanisms. The fact that many of the known canonical markers for all the cell types in the neocortex are TFs underscores their critical role in neurogenesis and the importance of their tightly controlled cell type-specific expression.

Dysregulation of gene-regulatory mechanisms underlies neuropsychiatric disease. Genetic association studies are beginning to comprehensively identify loci linked to specific brain traits and carrying risk for neuropsychiatric disease (Adams et al., 2016; Demontis et al., 2019; Ho et al., 2016; Kundaje et al., 2015; Okbay, Baselmans, et al., 2016; Okbay, Beauchamp, et al., 2016; Robinson et al., 2016). Yet, as most of this genetic variation falls in poorly annotated non-coding regions of the genome often regulating gene expression, a major challenge is to translate these findings into tractable biological processes. The emergence of genomic tools to profile gene expression and chromatin dynamics in single cells has facilitated the study of the interplay between gene regulatory elements and the TFs acting on these sites.

1.2 Foundational studies from our research group

1.2.1 Primary human neural progenitor cells: A robust *in vitro* model of corticogenesis

Dysregulation during embryonic development accounts for the majority of congenital abnormalities (Silbereis et al., 2016), yet this period is relatively understudied due to limited access to the tissue and until recently valid experimental models. Our ability to understand human neurodevelopmental disorders is limited by lack of access to physiologically relevant experimental models with which to study the dynamics of neurogenesis, lineage specification,

and cortical lamination. Previous cross-species comparisons have found different types and proportions of neural progenitors and cortical cell types, different time courses of progenitor proliferation and differentiation, and human-specific gene expression signatures during neurodevelopment (Bae et al., 2015; Bystron et al., 2008; Geschwind & Rakic, 2013; Lui et al., 2011; Sun & Hevner, 2014; Taverna et al., 2014). It is therefore imperative to employ models that reliably recapitulate the cellular and molecular composition of the human neocortex.

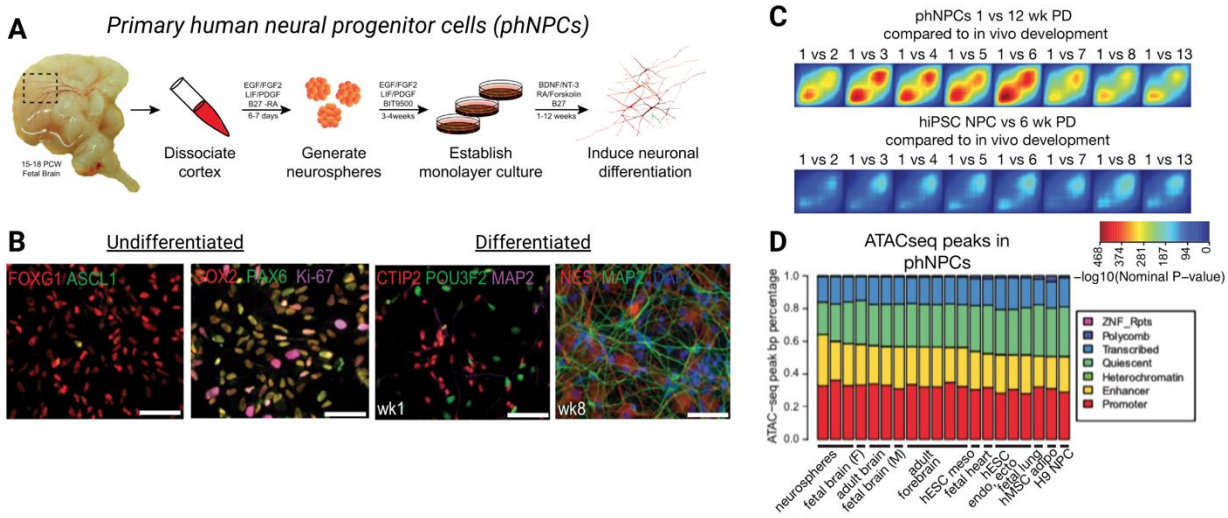

Figure 1.1: Human neural stem cell model of neocortical development. *Stein et al., 2014*
A) Isolation, culture, and differentiation of phNPCs B) phNPCs express dorsal telencephalic and cortical laminar makers and display stereotypical neuronal morphogenesis. C) Top: Transition mapping shows strong overlap between phNPCs and cortex up to late-mid fetal time points. Bottom: Overlap between hIPSC-derived NPCs differentiated for 6 weeks and in vivo brain is much lower D) ATAC-seq peaks from phNPCs overlap well with GREs in fetal brain (Liang et al., 2021).

To develop such a model, our research group has generated primary human neural progenitor cells (phNPCs) alongside a quantitative framework to assess how robustly phNPCs mimic neurogenesis and early cortical development up to mid-gestation time points (Stein et al., 2014). Upon differentiation, phNPCs can be used to model human corticogenesis *in vitro* with greater fidelity than human pluripotent neural stem cell systems. The vast majority of genes expressed in phNPCs fall within *in vivo* preserved gene expression modules, including modules enriched in radial glial and neuronal markers and those related to progenitor differentiation, chromatin remodeling, neuronal migration, axon and dendrite growth and synaptogenesis (Figure 1.1; Stein et al., 2014). Further, phNPCs provide a platform to study the non-coding genome, and up to 70% of *in vivo* detected from ATAC-seq peaks (assay for transposase-accessible chromatin with sequencing; de la Torre-Ubieta et al., 2018) are preserved in phNPCs. The genetically accessible nature of phNPCs has facilitated studies that functionally interrogate GREs in cortical neurogenesis and disease (de la Torre-Ubieta et al., 2018; Won et al., 2016) to uncover gene regulatory mechanisms of neocortical expansion, autism spectrum disorders, and schizophrenia (de la Torre-Ubieta et al., 2018; Won et al., 2016; Bae et al., 2015; Geschwind & Rakic, 2013; de la Torre-Ubieta et al., 2016; Gandal et al., 2018).

1.2.2 Exploring the epigenetic landscape of human neurogenesis

Human corticogenesis is coordinated by gene expression programs regulated by transcription factors and associated regulatory protein complexes within neural stem cells. Uncovering the precise roles and mechanisms of the diversity of relevant transcription factors is paramount to understanding both the fundamental principles of gene regulation and the biology of neuropsychiatric disorders. To address this, our laboratory mapped gene-enhancer pairs in

developing human neocortex supported by both evidence of functional correlation of chromatin accessibility (ATAC-seq peaks) between gene promoters and distal regulatory elements, and by physical interaction between these elements as assessed by Hi-C (chromosome conformation capture with deep sequencing; de la Torre-Ubieta et al., 2018).

1.3 Transcription factor ZFHX4: A candidate regulator of neurogenesis

1.3.1 Preliminary data

In the developing neocortex, differential TF activity specifies cell type identity by progressively restricting progenitor lineages and coordinating gene expression within maturing post-mitotic neurons (Lodato & Arlotta, 2015; Nord & West, 2020; Pollen et al., 2015; Xu et al., 2014). We have used our atlas of single-cell gene expression to identify novel TFs that specify neural progenitor and early neuron cell fates (Polioudakis et al., 2019).

Among these TFs we discovered that the Zinc Finger Homeobox 4 (ZFHX4) was uniquely expressed in neural progenitors and enriched in ventricular radial glia (vRG), a finding validated by RNA fluorescence in situ hybridization (FISH) (Figure 1.2). Ventricular radial glia give rise to the excitatory neurons and astrocytes of the human neocortex through a series of transition states and progenitor populations including outer radial glia and intermediate progenitor cells (Lui et al., 2011; Taverna et al., 2014). The mechanisms regulating this process are thought to control the size and thickness of the neocortex, ultimately responsible for its evolutionary expansion.

To profile gene expression and chromatin structure in the developing human neocortex, previous work from our lab generated the first combined atlas of gene expression and chromatin structure using bulk ATAC-seq and Hi-C from micro-dissected lamina. This atlas of neocortical GREs revealed putative ZFHX4 enhancers with increased accessibility in the neural progenitor-enriched GZ as compared to the neuron-enriched cortical plate (CP). Overall, preliminary data from our research group reports that ZFHX4 is a TF with enriched expression within neural progenitors of the developing human neocortex and identified ZFHX4 GREs predicted to drive gene expression programs during neurogenesis.

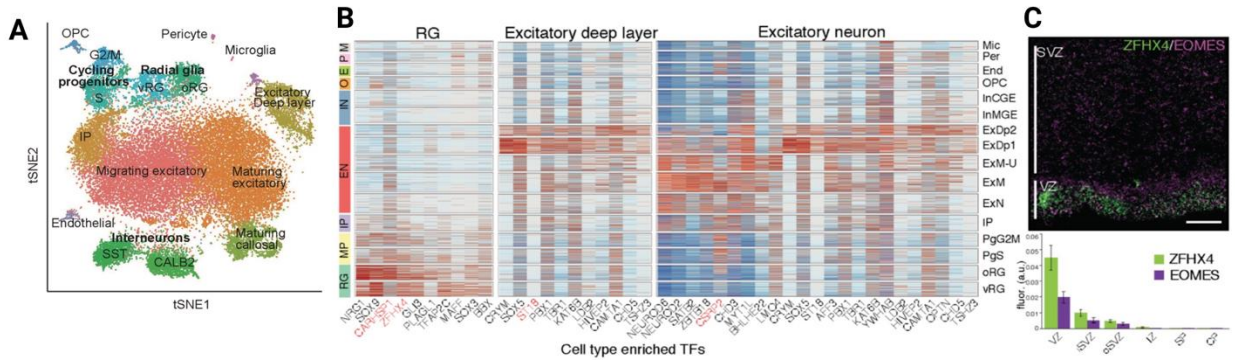

Figure 1.2: ZFHX4 is a candidate regulatory TF for human corticogenesis
A) tSNE plot showing distinct cell type clusters identified in neocortex from scRNAseq analysis.
B) Heatmap depicting the expression of TFs in the cortex. ZFHX4 is enriched in RG and MP
C) Validation of ZFHX4 expression in the VZ and SVZ by RNA-FISH

1.3.2 Association with neurodevelopmental disorders

ZFHX4 has been implicated in several neurodevelopmental disorders including 8q21.11 microdeletion syndrome (Palomares et al., 2011). This study detected the deletion of only one protein-coding gene, ZFHX4, across eight patients with 8q21.11 microdeletion syndrome, suggesting that ZFHX4 participates in the developmental processes that are disrupted in this disorder. Additional disorders that ZFHX4 has been associated with in the literature are listed below (Table 1.1) and include syndromic Peters anomaly (Happ, 2016), childhood apraxia of speech (Eising et al., 2019) and congenital bilateral isolated ptosis (McMullan et al., 2002).

Table 1.1: Neurodevelopmental disorders associated with ZFHX4. Listed publications have linked chromosomal/genetic aberrations coinciding with ZFHX4's coding region to various neurodevelopmental disorders. Participant demographics and diagnoses are also summarized.

Disorder name	Symptoms	Clinical screen	Patient demographics	Chromosomal/ genetic aberrations
Syndromic Peters anomaly *(Happ, 2016)*	Global developmental delay; Intellectual disability; Speech impairment; Impaired visual acuity; Facial dysmorphisms; Microphthalmia; Central white matter volume loss; Thin corpus callosum	Whole exome sequencing; Chromosomal microarray analyses	N = 2; Sex: 1M, 1F; Age: 4mo – 6yrs	Submicroscopic deletions of 8q21.11 (1.4-13.1 Mb)
8q21.11 microdeletion syndrome *(Palomares et al., 2011)*	Global developmental delay; Ptosis; Intellectual disability; Hypotonia; Decreased balance; Sensorineural hearing loss; Impaired visual acuity; Facial dysmorphisms; Digital malformations	High-resolution oligonucleotide array	N = 8; Sex: 4M, 4F Age: 1mo – 17yrs	Submicroscopic deletions of 8q21.11 (0.7-13.6 Mb)
Childhood apraxia of speech *(Eising et al., 2019)*	Intellectual disability; Severe speech delay; Hypotonia; Facial dysmorphism	Whole-genome sequencing and variant calling	N = 19; Sex: 8M, 11F Age: 13-19 yrs	Novel LOF variants affecting several genes, including ZFHX4
Congenital bilateral isolated ptosis *(McMullan et al., 2002)*	Ptosis	Conventional cytogenetics	N = 1; Sex: M Age: 25yrs	*De novo* balanced translocation disrupting ZFHX4

1.3.3 Role in cell proliferation and differentiation: Current theories and models

TF interactions with co-activator, co-repressor and/or chromatin remodeling complexes have been shown to regulate cortical neurogenesis. Indeed, studies in glioblastoma tumor-initiating cells (GBM TICs) have demonstrated that ZFHX4 is a master regulator of CHD4 (Chudnovsky et al., 2014), a core member of the nucleosome remodeling and deacetylase

(NuRD) complex implicated in neurogenesis (Yoo & Crabtree, 2009). The depletion of ZFHX4 expression reduces the proliferative capacity and plasticity of GBM TICs. Additionally, analysis of the NuRD complex during mouse corticogenesis reported that the subunits CHD4, CHD5, and CHD3 are recruited sequentially and operate mutually exclusively of each other to coordinate the transitions from basal progenitor proliferation, early radial migration, and late migration and neuronal laminar specification, respectively (Nitarska, 2016).

Chromatin immunoprecipitation with sequencing (ChIP-seq) of ZFHX4 and of CHD4 in GBM cell lines revealed partially overlapping genomic targets (Chudnovsky et al., 2014), suggesting at least partly independent downstream mechanisms and underscoring the need to perform these studies to define the contribution of each protein in downstream regulatory cascades. ZFHX4's role in maintaining stemness in both mouse neurodevelopment and GBM TICs may indicate a role for ZFHX4 in neuronal development.

Given these results (Chudnovsky et al., 2014), we can expect that some of ZFHX4 mechanisms occur through its interaction with the NuRD complex. Currently, there has been no systematic characterization of the structural domains necessary for this interaction. ZFHX4 has four homeodomains and 22-finger domains (Hemmi et al., 2006), which are predicted to mediate DNA-protein interactions but not necessarily interactions with other proteins. An analysis of ZFHX4 protein sequence using protein domain databases and prediction tools at high stringency (UniProt, ScanSite 4.0) identified several domains known to mediate protein-protein interactions including four Proline rich domains and three Src homology 3 (SH3) group domains. The predicted structure of ZFHX4, as viewed on the AlphaFold Protein Structure Database (Figure 1.3; Varadi et al., 2024; Jumper et al., 2021).

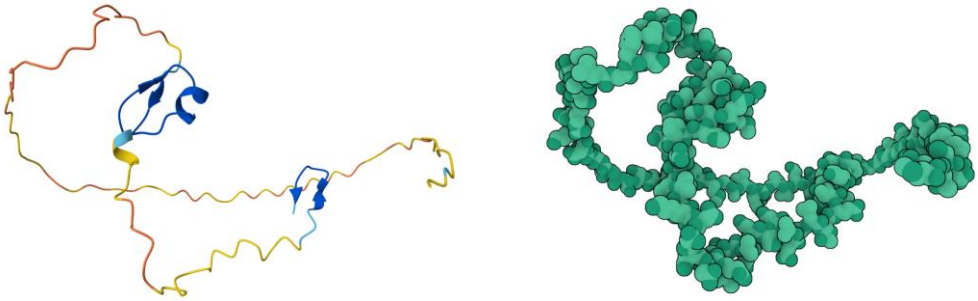

Figure 1.3: Predicted ZFHX4 structure. Stylized (left) and illustrative (right) views of the predicted structure of *Homo Sapiens* ZFHX4 (UniProt ID: E5RGK3).

1.4 Questions Addressed in this Study

Here, I outline my efforts to advance functional interpretation of transcriptomic and epigenomic annotations of the developing neocortex and characterize the role of ZFHX4, a TF with uncharacterized roles in brain development. Using CRISPR-Cas9 genomic engineering, I knocked down ZFHX4 expression in phNPCs, a highly scalable and validated *in vitro* model of human cortical development. ZFHX4 depletion led to the dysregulation of neurogenesis, as measured by immunocytochemical assessment of cell type identity via canonical markers. I then interrogated the molecular mechanisms regulating ZFHX4 by identifying three putative gene regulatory elements and reported that targeting these GREs via CRISPR-interference (CRISRPi) led to changes in neural progenitor specification. These observations not only support my hypothesis that ZFHX4 contributes to maintaining the stemness of neural progenitor cells, but also demonstrate the validity of using CRISPRi methods to interrogate TF regulation.

Additionally, I have begun developing an experimental pipeline to study gene-regulatory functions in an *in vivo* model (organotypic slice culture) to complement our well-characterized *in vitro* model (phNPCs). Overall, my efforts to characterize the role of ZFHX4 in a human corticogenesis model have contributed to the development of an experimental framework that

can be leveraged to interrogate the role of additional candidate TFs in complementary *in vivo* and *in vitro* models of corticogenesis. Acquiring a more complete understanding of gene regulatory mechanisms that orchestrate neurogenesis, including *cis*-regulatory elements and transcription factors operating at these loci, will provide insights into molecular mechanisms generating human cognitive capabilities and their dysregulation in neuropsychiatric disease.

References

Adams, H. H. H., Hibar, D. P., Chouraki, V., Stein, J. L., Nyquist, P. A., Rentería, M. E., Trompet, S., Arias-Vasquez, A., Seshadri, S., Desrivières, S., Beecham, A. H., Jahanshad, N., … Thompson, P. M. (2016). Novel genetic loci underlying human intracranial volume identified through genome-wide association. *Nature Neuroscience*, *19*(12), 1569–1582. https://doi.org/10.1038/nn.4398

Amano, T., Sagai, T., Tanabe, H., Mizushina, Y., Nakazawa, H., & Shiroishi, T. (2009). Chromosomal dynamics at the Shh locus: Limb bud-specific differential regulation of competence and active transcription. *Dev. Cell*, *16*, 47–57.

Arnold, S. J., Huang, G.-J., Cheung, A. F. P., Era, T., Nishikawa, S.-I., Bikoff, E. K., Molnár, Z., Robertson, E. J., & Groszer, M. (2008). The T-box transcription factor Eomes/Tbr2 regulates neurogenesis in the cortical subventricular zone. *Genes & Development*, *22*(18), 2479–2484. https://doi.org/10.1101/gad.475408

Baala, L., Briault, S., Etchevers, H. C., Laumonnier, F., Natiq, A., Amiel, J., Boddaert, N., Picard, C., Sbiti, A., Asermouh, A., Attié-Bitach, T., Encha-Razavi, F., Munnich, A., Sefiani, A., & Lyonnet, S. (2007). Homozygous silencing of T-box transcription factor EOMES leads to microcephaly with polymicrogyria and corpus callosum agenesis. *Nature Genetics*, *39*(4), 454–456. https://doi.org/10.1038/ng1993

Bae, B., Jayaraman, D., & Walsh, C. A. (2015). Genetic Changes Shaping the Human Brain. *Developmental Cell*, *32*(4), 423–434. https://doi.org/10.1016/j.devcel.2015.01.035

Bystron, I., Blakemore, C., & Rakic, P. (2008). Development of the human cerebral cortex: Boulder Committee revisited. *Nat. Rev. Neurosci*, *9*, 110–122.

Chudnovsky, Y., Kim, D., Zheng, S., Whyte, W. A., Bansal, M., Bray, M.-A., Gopal, S., Theisen, M. A., … Chheda, M. G. (2014). ZFHX4 interacts with the NuRD core member CHD4 and regulates the glioblastoma tumor initiating cell state. *Cell Reports*, *6*(2), 313–324. https://doi.org/10.1016/j.celrep.2013.12.032

Day, J. J., & Sweatt, J. D. (2011). Epigenetic mechanisms in cognition. *Neuron*, *70*, 813–829.

de la Torre-Ubieta, L., Stein, J. L., Won, H., Opland, C. K., Liang, D., Lu, D., & Geschwind, D. H. (2018). The Dynamic Landscape of Open Chromatin during Human Cortical Neurogenesis. *Cell*, *172*(1–2), 289-304.e18. https://doi.org/10.1016/j.cell.2017.12.014

de la Torre-Ubieta, L., Won, H., Stein, J. L., & Geschwind, D. H. (2016). Advancing the understanding of autism disease mechanisms through genetics. *Nature Medicine*, *22*, 345–361.

Demontis, D., Walters, R. K., Martin, J., Mattheisen, M., Als, T. D., Agerbo, E., Baldursson, G., Belliveau, R., Bybjerg-Grauholm, J., & Bækvad-Hansen, M. (2019). Discovery of the

first genome-wide significant risk loci for attention deficit/hyperactivity disorder. *Nature Genetics*, *51*, 63–75.

Eising, E., Carrion-Castillo, A., Vino, A., Strand, E. A., Jakielski, K. J., Scerri, T. S., Hildebrand, M. S., Webster, R., Ma, A., Mazoyer, B., Francks, C., Bahlo, M., Scheffer, I. E., Morgan, A. T., Shriberg, L. D., & Fisher, S. E. (2019). A set of regulatory genes co-expressed in embryonic human brain is implicated in disrupted speech development. *Molecular Psychiatry*, *24*(7), 1065–1078. https://doi.org/10.1038/s41380-018-0020-x

Gandal, M. J., Leppa, V., Won, H., Parikshak, N. N., & Geschwind, D. H. (2016). The road to precision psychiatry: Translating genetics into disease mechanisms. *Nature Neuroscience*, *19*(11), 1397–1407. https://doi.org/10.1038/nn.4409

Gandal, M. J., Zhang, P., Hadjimichael, E., Walker, R. L., Chen, C., Liu, S., Won, H., van Bakel, H., Varghese, M., Wang, Y., Shieh, A. W., Haney, J., Parhami, … Geschwind, D. H. (2018). Transcriptome-wide isoform-level dysregulation in ASD, schizophrenia, and bipolar disorder. *Science*, *362*(6420), eaat8127. https://doi.org/10.1126/science.aat8127

Geschwind, D. H., & Rakic, P. (2013). Cortical evolution: Judge the brain by its cover. *Neuron*, *80*, 633–647.

Happ. (2016). 8q21.11 Microdeletion in Two Patients with Syndromic Peters Anomaly. *Am J Med Genet A*, *170*(9), 2471–2475.

Hemmi, K., Ma, D., Miura, Y., Kawaguchi, M., Sasahara, M., Hashimoto-Tamaoki, T., Tamaoki, T., Sakata, N., & Tsuchiya, K. (2006). A homeodomain-zinc finger protein, ZFHX4, is expressed in neuronal differentiation manner and suppressed in muscle differentiation manner. *Biological and Pharmaceutical Bulletin*, *29*, 1830–1835.

Ho, Y. Y. W., Evans, D. M., Montgomery, G. W., Henders, A. K., Kemp, J. P., Timpson, N. J., St Pourcain, B., Heath, A. C., Madden, P. A. F., Loesch, D. Z., McNevin, D., Daniel, R., Davey-Smith, G., Martin, N. G., & Medland, S. E. (2016). Common Genetic Variants Influence Whorls in Fingerprint Patterns. *The Journal of Investigative Dermatology*, *136*(4), 859–862. https://doi.org/10.1016/j.jid.2015.10.062

Jakovcevski, M., & Akbarian, S. (2012). Epigenetic mechanisms in neurological disease. *Nature Med*, *18*, 1194–1204.

Jumper, J., Evans, R., Pritzel, A., Green, T., Figurnov, M., Ronneberger, O., Tunyasuvunakool, K., Bates, R., Žídek, A., Potapenko, A., Bridgland, A., Meyer, C., Kohl, S. A. A., Ballard, A. J., Cowie, A., Romera-Paredes, B., Nikolov, S., Jain, R., Adler, J., … Hassabis, D. (2021). Highly accurate protein structure prediction with AlphaFold. *Nature*, *596*(7873), 583–589. https://doi.org/10.1038/s41586-021-03819-2

Kang, H. J., Kawasawa, Y. I., Cheng, F., Zhu, Y., Xu, X., Li, M., Sousa, A. M. M., Pletikos, M., Meyer, K. A., Sedmak, G., Guennel, T., Shin, Y., Johnson, M. B., Krsnik, Ž., Mayer, S., … Šestan, N. (2011). Spatio-temporal transcriptome of the human brain. *Nature*, *478*(7370), 483–489. https://doi.org/10.1038/nature10523

Krasnegor, N. A., Lyon, G. R., & Goldman-Rakic, P. S. (1997). *Development of the Prefrontal Cortex: Evolution, Neurobiology, and Behavior*. P.H. Brookes Publishing Company.

Kundaje, A., Meuleman, W., Ernst, J., Bilenky, M., Yen, A., Heravi-Moussavi, A., Kheradpour, P., Zhang, Z., Wang, J., Ziller, M. J., Amin, V., Whitaker, J. W., Schultz, M. D., Ward, L., … Kellis, M. (2015). Integrative analysis of 111 reference human epigenomes. *Nature*, *518*(7539), 317–330. https://doi.org/10.1038/nature14248

Lodato, S., & Arlotta, P. (2015). Generating neuronal diversity in the mammalian cerebral cortex. *Annual Review of Cell and Developmental Biology*, *31*, 699–720. https://doi.org/10.1146/annurev-cellbio-100814-125353

Lui, J. H., Hansen, D. V., & Kriegstein, A. R. (2011). Development and evolution of the human neocortex. *Cell*, *146*, 18–36.

McMullan, T. W., Crolla, J. A., Gregory, S. G., Carter, N. P., Cooper, R. A., Howell, G. R., & Robinson, D. O. (2002). A candidate gene for congenital bilateral isolated ptosis identified by molecular analysis of a de novo balanced translocation. *Human Genetics*, *110*(3), 244–250. https://doi.org/10.1007/s00439-002-0679-5

Mehler M. F. (2008). Epigenetics and the nervous system. *Ann Neurol*, *64*, 602–617.

Miller, J. A., Ding, S.-L., Sunkin, S. M., Smith, K. A., Ng, L., Szafer, A., Ebbert, A., Riley, Z. L., Royall, J. J., Aiona, K., Arnold, J. M., Bennet, C., Bertagnolli, D., Brouner, K., … Lein, E. S. (2014). Transcriptional landscape of the prenatal human brain. *Nature*, *508*(7495), 199–206. https://doi.org/10.1038/nature13185

Nitarska. (2016). A Functional Switch of NuRD Chromatin Remodeling Complex Subunits Regulates Mouse Cortical Development. *Cell Reports*, *17*, 1683–1698.

Nord, A. S., Pattabiraman, K., Visel, A., & Rubenstein, J. L. R. (2015). Genomic perspectives of transcriptional regulation in forebrain development. *Neuron*, *85*(1), 27–47. https://doi.org/10.1016/j.neuron.2014.11.011

Nord, A. S., & West, A. E. (2020). Neurobiological functions of transcriptional enhancers. *Nature Neuroscience*, *23*(1), 5–14. https://doi.org/10.1038/s41593-019-0538-5

Okbay, A., Baselmans, B. M. L., Neve, J. E., Turley, P., Nivard, M. G., Fontana, M. A., Meddens, S. F. W., Linnér, R. K., Rietveld, C. A., & Derringer, J. (2016). Genetic variants associated with subjective wellbeing, depressive symptoms, and neuroticism identified through genome-wide analyses. *Nature Genetics*, *48*, 624–633.

Okbay, A., Beauchamp, J. P., Fontana, M. A., Lee, J. J., Pers, T. H., Rietveld, C. A., Turley, P., Chen, G.-B., Emilsson, V., Meddens, S. F. W., Oskarsson, S., Pickrell, J. K., Thom, K., … Benjamin, D. J. (2016). Genome-wide association study identifies 74 loci associated with educational attainment. *Nature*, *533*(7604), 539–542. https://doi.org/10.1038/nature17671

Palomares, M., Delicado, A., & Mansilla, E. (2011). Characterization of a 8q21.11 microdeletion syndrome associated with intellectual disability and a recognizable phenotype. *Am J Hum Genet*, *89*, 295–301.

Pollen, A. A., Nowakowski, T. J., Chen, J., Retallack, H., Sandoval-Espinosa, C., Nicholas, C. R., Shuga, J., Liu, S. J., Oldham, M. C., Diaz, A., Lim, D. A., Leyrat, A. A., West, J. A., & Kriegstein, A. R. (2015). Molecular identity of human outer radial glia during cortical development. *Cell*, *163*(1), 55–67. https://doi.org/10.1016/j.cell.2015.09.004

Patowary, A., Zhang, P., Jops, C., Vuong, C. K., Ge, X., Hou, K., Kim, M., Gong, N., Margolis, M., Vo, D., Wang, X., Liu, C., Pasaniuc, B., Li, J. J., Gandal, M. J., & Torre-Ubieta, L. de la. (2023). *Cell-type-specificity of isoform diversity in the developing human neocortex informs mechanisms of neurodevelopmental disorders* (p. 2023.03.25.534016). bioRxiv. https://doi.org/10.1101/2023.03.25.534016

Polioudakis, D., de la Torre-Ubieta, L., Langerman, J., Elkins, A. G., Shi, X., Stein, J. L., Vuong, C. K., Nichterwitz, S., Gevorgian, … Geschwind, D. H. (2019). A Single-Cell Transcriptomic Atlas of Human Neocortical Development during Mid-gestation. *Neuron*, *103*(5), 785-801.e8. https://doi.org/10.1016/j.neuron.2019.06.011

Robinson, E. B., St Pourcain, B., Anttila, V., Kosmicki, J. A., Bulik-Sullivan, B., Grove, J., Maller, J., Samocha, K. E., … Daly, M. J. (2016). Genetic risk for autism spectrum disorders and neuropsychiatric variation in the general population. *Nature Genetics*, *48*(5), 552–555. https://doi.org/10.1038/ng.3529

Shain, A. H., & Pollack, J. R. (2013). The spectrum of SWI/SNF mutations, ubiquitous in human cancers. *PloS One*, *8*(1), e55119. https://doi.org/10.1371/journal.pone.0055119

Silbereis, J. C., Pochareddy, S., Zhu, Y., Li, M., & Sestan, N. (2016). The Cellular and Molecular Landscapes of the Developing Human Central Nervous System. *Neuron*, *89*(2), 248–268. https://doi.org/10.1016/j.neuron.2015.12.008

Siletti, K., Hodge, R., Mossi Albiach, A., Lee, K. W., Ding, S.-L., Hu, L., Lönnerberg, P., Bakken, T., Casper, T., Clark, M., Dee, N., Gloe, J., … Linnarsson, S. (2023). Transcriptomic diversity of cell types across the adult human brain. *Science (New York, N.Y.)*, *382*(6667), eadd7046. https://doi.org/10.1126/science.add7046

Stein, J. L., de la Torre-Ubieta, L., Tian, Y., Parikshak, N. N., Hernández, I. A., Marchetto, M. C., Baker, D. K., Lu, D., Hinman, C. R., Lowe, J. K., Wexler, E. M., Muotri, A. R., Gage, F. H., Kosik, K. S., & Geschwind, D. H. (2014). A Quantitative Framework to Evaluate

Modeling of Cortical Development by Neural Stem Cells. *Neuron*, *83*(1), 69–86. https://doi.org/10.1016/j.neuron.2014.05.035

Sun, T., & Hevner, R. F. (2014). Growth and folding of the mammalian cerebral cortex: From molecules to malformations. *Nature Reviews Neuroscience*, *15*(4), 217–232. https://doi.org/10.1038/nrn3707

Taverna, E., Götz, M., & Huttner, W. B. (2014). The cell biology of neurogenesis: Toward an understanding of the development and evolution of the neocortex. *Annual Review of Cell and Developmental Biology*, *30*, 465–502. https://doi.org/10.1146/annurev-cellbio-101011-155801

van Bokhoven, H. (2011). Genetic and epigenetic networks in intellectual disabilities. *Annual Review of Genetics*, *45*, 81–104. https://doi.org/10.1146/annurev-genet-110410-132512

Varadi, M., Bertoni, D., Magana, P., Paramval, U., Pidruchna, I., Radhakrishnan, M., Tsenkov, M., Nair, S., Mirdita, M., Yeo, J., Kovalevskiy, O., Tunyasuvunakool, K., Laydon, A., Žídek, … Velankar, S. (2024). AlphaFold Protein Structure Database in 2024: Providing structure coverage for over 214 million protein sequences. *Nucleic Acids Research*, *52*(D1), D368–D375. https://doi.org/10.1093/nar/gkad1011

Wilson, B. G. (2008). Epigenetic antagonism between polycomb and SWI/SNF complexes during oncogenic transformation. *Cancer Cell*, *18*, 316–328.

Won, H., Torre-Ubieta, L., Stein, J. L., Parikshak, N. N., Huang, J., Opland, C. K., Gandal, M. J., Sutton, G. J., Hormozdiari, F., & Lu, D. (2016). Chromosome conformation elucidates regulatory relationships in developing human brain. *Nature*, *538*, 523–527.

Xu, X., Wells, A. B., O'Brien, D. R., Nehorai, A., & Dougherty, J. D. (2014). Cell type-specific expression analysis to identify putative cellular mechanisms for neurogenetic disorders. *Journal of Neuroscience*, *34*, 1420–1431.

Yoo, A. S., & Crabtree, G. R. (2009). ATP-dependent chromatin remodeling in neural development. *Curr Opin Neurobio*, *19*, 120–126.

Ziffra, R. S., Kim, C. N., Ross, J. M., Wilfert, A., Turner, T. N., Haeussler, M., Casella, A. M., Przytycki, P. F., Keough, K. C., Shin, D., Bogdanoff, D., Kreimer, A., Pollard, K. S., Ament, S. A., Eichler, E. E., Ahituv, N., & Nowakowski, T. J. (2021). Single-cell epigenomics reveals mechanisms of human cortical development. *Nature*, *598*(7879), 205–213. https://doi.org/10.1038/s41586-021-03209-8

Chapter 2: Materials and Methods

2.1 CRISPR(i) constructs

2.1.1 Lentiviral vectors

Three lentiviral vectors provided the backbones for the clones used in this study (Figure 2.1). Lentiviral vectors do not require the use of a transfection reagent, which can affect the biology of target cells, and effectively transduce most mammalian cell lines including primary or stem cells (Heckl et al., 2014). They stably integrate in the host genome, leading to long-term expression that persists through proliferation of transduced cells. In addition, their large packaging capacity allows simultaneous delivery of both the Cas9 enzyme and small guide RNAs (sgRNAS).

i. pL-CRISPR.EFS.tRFP

Standard Clustered regularly interspaced short palindromic repeat (CRISPR) experiments targeting ZFHX4 exon 2 were cloned into a vector with CRISPR-Cas9 delivery for *S. pyogenes* Cas9 (SpCas9), sgRNA scaffold flanked by BsmBI restriction enzyme cleavage sites. The vector contains a human short EF1alpha (EFS) promoter and co-expresses the fluorescent reporter gene tagRFP via a P2A ribosome-skipping cleavage site.

ii. pLV hU6-sgRNA hUbC-dCas9-KRAB-T2a-GFP

CRISPR-interference (CRISPRi) experiments were conducted in a vector backbone containing catalytically inactive Cas9 (dCas9) fused to a Krüppel-associated box KRAB transcriptional repressor (dCas9-KRAB). The KRAB domain contains the C2H2 zinc finger domain, KOX1. CRISPRi enacts highly specific and reversible transcriptional repression without introducing mutations to the genome. The vector's fluorescent reporter gene, eGFP, is linked through a P2A ribosome-skipping site and driven by a human UbiquitinC promoter (Parsi

et al., 2017; Thakore et al., 2015). The sgRNA scaffold is flanked by BsmBI restriction enzyme cleavage sites.

iii. pLV hU6-sgRNA.CapSeq hUbC-dCas9-KRAB.ZIM3-T2a-GFP

The CRISPRi cassette was modified to attach a "capture sequence" compatible with scRNAseq to the sgRNA scaffold (Replogle et al., 2020) to allow direct capture of both the expressed sgRNA and endogenous mRNAs from each cell during 10X genomics. The KRAB domain was changed from KOX1 to ZIM3, the latter which was reported to repress gene expression with ten-fold more potency than the former (Alerasool et al., 2020).

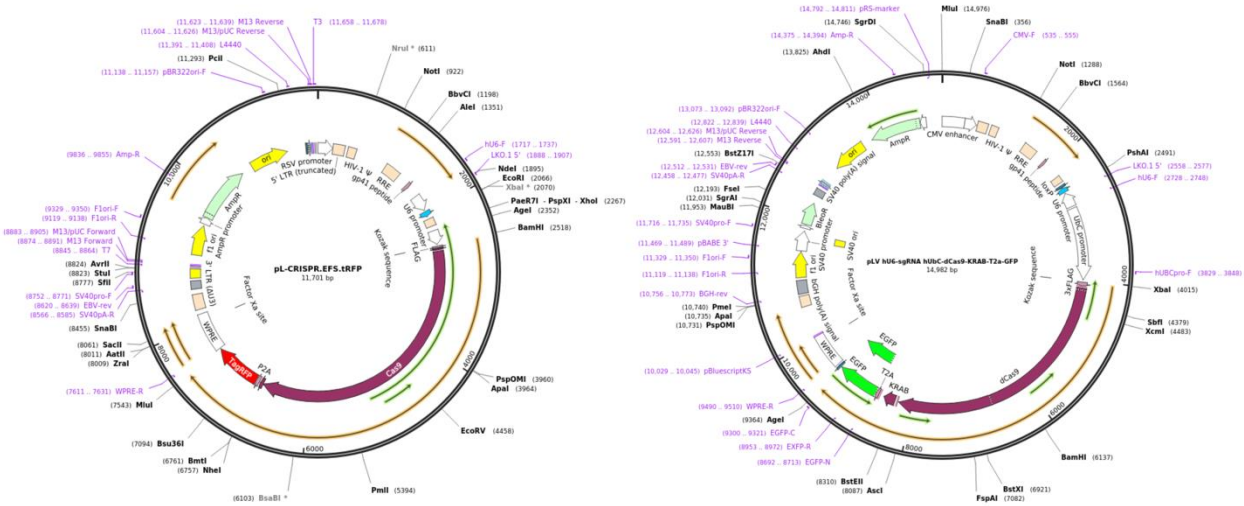

Figure 2.1: Lentiviral backbones. Left, **pL-CRISPR.EFS.tRFP** (addgene.org/57819). Heckl et al Nat Biotechnol. 2014 Jun 22. doi: 10.1038/nbt.2951. Right, pLV hU6-sgRNA hUbC-dCas9-KRAB-T2a-GFP. (addgene.org/71237) Thakore et al Nat Methods. 2015 Dec;12(12):1143-9. doi: 10.1038/nmeth.3630. Epub 2015 Oct 26.

2.1.2 Guide RNAs

sgRNA sequences, the vectors they were cloned into, and their genomic targets are listed in Table 2.1 and Table 2.2.

Table 2.1: CRISPR(i) clones and their genomic targets including differential regulatory elements (DREs). Reference genome: UCSC Genome Browser (GRCH37/19).

ZFHX4 sgRNA	Target ATAC peak	Target ZFX4 GRE/Exon	sgRNA target
pLV hU6-sgRNA hUbC-dCas9-KRAB-T2a-GFP			
Promoter 1	chr8.77592526-77597752	ATAC: GZ>CP	chr8.77593601-77593620
Promoter 2	chr8.77687258-77689292	Annotated promoter (Hi-C: DRE interaction)	chr8.77688207-77688226
DRE_1	chr8.77597867-77602324	ATAC: GZ>CP (Hi-C: Promoter 2 interaction)	chr8.77600104-77600123
DRE_2	chr8.77597867-77602324	ATAC: GZ>CP (Hi-C: Promoter 2 interaction)	chr8.77600046-77600065
pLV hU6-sgRNA.CapSeq hUbC-dCas9-KRAB.ZIM3-T2a-GFP			
Promoter 1	chr8.77592526-77597752	ATAC: GZ>CP	chr8.77593601-77593620
Promoter 2	chr8.77687258-77689292	Annotated promoter (Hi-C: DRE interaction)	chr8.77688207-77688226
DRE_1	chr8.77597867-77602324	ATAC: GZ>CP (Hi-C: Promoter 2 interaction)	chr8.77600104-77600123
DRE_2	chr8.77597867-77602324	ATAC: GZ>CP (Hi-C: Promoter 2 interaction)	chr8.77600104-77600123
TSS.A	-----	Exon 2	chr8: 77593658 - 77593677
TSS.B	-----	Exon 2	chr8: 77593997 - 77594016
pL-CRISPR.EFS.tRFP			
Exon2.Gilbert	-----	Exon 2	chr8:77616550-77616573
Exon2.1	-----	Exon 2	chr8: 77616688-77616708
Exon2.2	-----	Exon 2	chr8: 77617273-77617292

2.1.3 Cloning

Cloning was performed using the NEBuilder HiFi DNA Assembly cloning method (New England Biolabs). Reverse- and forward- sgRNA sequences were ordered as single stranded oligonucleotides from Integrated DNA Technologies. Oligonucleotide pairs were phosphorylated and annealed at 75C in a thermal cycler. Lentiviral (LV) vectors were cut with the restriction digest enzyme BsmbI, dephosphorylated, then underwent DNA electrophoresis in an 0.8% agarose gel. Linearized vectors were extracted from the gel, purified (Takara PCR cleanup and gel extraction kit) and the concentration of extracted DNA was measured by nanodrop. Cut vectors and the annealed oligo inserts were ligated (Roche Rapid Ligation Kit) with *a* DNA concentration ratio of 1:3 (50 ng:150ng) then transformed into chemically competent *E. coli* (Invitrogen, One Shot Stbl3). Transformants were plated onto ampicillin-selection LB-agar plates and incubated at 37 C overnight. Colonies were picked the next day, cultured overnight, then harvested for plasmid DNA (QIAprep Spin Miniprep Kit). Plasmids were purified (QIAGEN PCR-purification kit) and sent to RetroGen Inc. for sequencing. Sequencing primers are listed below (Table 2.2). Sequence-validated plasmids were extracted and purified (QIAGEN Plasmid MaxiPrep Kit).

For lentiviral production, human embryonic kidney (HEK293) cells were transfected using polyethylenimine (PEI), a stable cationic polymer that binds plasmids to form positively charged particles that bind to anionic cell surfaces. This complex is endocytosed by host HEK cells to release the cloned plasmids into the cytoplasm. LV was concentrated from transfected HEK cells by 10% sucrose gradient centrifugation, suspended in PBS, aliquoted, and stored at -80C. The viral titer was measured (Takara Bio. Lenti-X qRT-PCR Titration Kit) and used to calculate multiplicity of infection (MOI) for downstream experiments.

To assess the editing efficiency of CRISPR sgRNAs designed to target ZFHX4 exon 2, primary human neural progenitor cells (phNPCs) were infected (1.5 MOI) with control and experimental CRISPR constructs and cultured under proliferative conditions for 3 days (phNPC culturing methods are detailed below: 2.2.1 Culturing phNPCs under proliferation and differentiation conditions). DNA was extracted and a ~500bp region flanking the targeted genomic insertion-deletions (indels) and PCR-amplified (Sigma-Aldrich *KOD Hot Start Xtreme DNA polymerase*). Amplicons were purified and sent for Sanger sequencing with a sequencing primer targeting ~150 bp upstream of the targeted indel. Amplifying and sequencing primers are listed below (Table 2.2). Control and experimental sequencing results were inputted into the Synthego Inference of CRISPR Edits (ICE) online tool to return predicted indel mutations and rate of knockdown.

To assess for changes in ZFHX4 expression at the mRNA level, phNPCs were infected, cultured, and harvested as described above. RNA was extracted from infected phNPCs (QIAZOL lysis and QIAGEN RNA Extraction Kit) and underwent complementary DNA (cDNA) synthesis (Invitrogen SuperScript III Reverse Transcriptase). RT qRT-PCR (Real-time quantitative reverse transcriptase polymerase chain reaction) was performed (Thermofisher SYBR Green real-time PCR master mix) in triplicate to assess for relative expression at the CRISPR-Cas9 targeted ZFHX4 locus between control and experimental constructs. RT-primers and their targets are listed below (Table 2.2).

Table 2.2: Primers and their experimental applications.

sgRNAs

ZFHX4 sgRNA	DNA oligonucleotide sequences	LV vector
Promoter 1	Fwd: CACCGCTCGCTGTTTGGTTGTGAAG Rev: AAACCTTCACAACCAAACAGCGAGC	pLV hU6-sgRNA hUbC-dCas9-KRAB-T2a-GFP
Promoter 2	Fwd: CACCGCCTGCTGTTCTTAACACAG Rev: AAACCTGTGTTAAGAACAGCAGGC	pLV hU6-sgRNA hUbC-dCas9-KRAB-T2a-GFP
DRE_1	Fwd: CACCGTATTGATAGAGGATTTGGAA Rev: AAACTTCCAAATCCTCTATCAATAC	pLV hU6-sgRNA hUbC-dCas9-KRAB-T2a-GFP
DRE_2	Fwd: CACCGAAGTATAATTATACTTGTGA Rev: AAACTCACAAGTATAATTATACTTC	pLV hU6-sgRNA hUbC-dCas9-KRAB-T2a-GFP
Promoter 1	Fwd: CACCGCTCGCTGTTTGGTTGTGAAG Rev: AAACCTTCACAACCAAACAGCGAGC	pLV hU6-sgRNA.CapSeq hUbC-dCas9-KRAB.ZIM3-T2a-GFP
Promoter 2	Fwd: CACCGCCTGCTGTTCTTAACACAG Rev: AAACCTGTGTTAAGAACAGCAGGC	pLV hU6-sgRNA.CapSeq hUbC-dCas9-KRAB.ZIM3-T2a-GFP
DRE_1	Fwd: CACCGTATTGATAGAGGATTTGGAA Rev: AAACTTCCAAATCCTCTATCAATAC	pLV hU6-sgRNA.CapSeq hUbC-dCas9-KRAB.ZIM3-T2a-GFP
DRE_2	Fwd: CACCGAAGTATAATTATACTTGTGA Rev: AAACTCACAAGTATAATTATACTTC	pLV hU6-sgRNA.CapSeq hUbC-dCas9-KRAB.ZIM3-T2a-GFP
TSS.A	Fwd: GGGCATGGAGCGGTCCTCGG Rev: AAACCCGAGGACCGCTCCATGCCC	pLV hU6-sgRNA.CapSeq hUbC-dCas9-KRAB.ZIM3-T2a-GFP
TSS.B	Fwd: GAGCAGGAGCGAGCGAGGTA Rev: AAACTACCTCGCTCGCTCCTGCTC	pLV hU6-sgRNA.CapSeq hUbC-dCas9-KRAB.ZIM3-T2a-GFP
Exon2.Gilbert	Fwd: CACCGTTGCAGGGTATCTCCTTTGCTG Rev: AAACCAGCAAAGGAGATACCCTGCAAC	pL-CRISPR.EFS.tRFP
Exon2.1	Fwd: CACCGTGACGTGGAAAATCTAACAG Rev: AAACCTGTTAGATTTTCCACGTCAC	pL-CRISPR.EFS.tRFP
Exon2.1	Fwd: CACCGCGTCTCCGCCATAATACAG Rev: AAACCTGTATTATGGCGGAGACGC	pL-CRISPR.EFS.tRFP

RT-qPCR

Target sgRNA	DNA oligonucleotide sequences
Promoter 2	Fwd: TACAACATGTCCGTTCGGTG Rev: CTCAACTGCTGCTCTGTAAG
DRE_1 DRE_2	Fwd: CGAAGATCGAGTAGGAACTG Rev: CTTGAGATAGGAGGGGAGTC
Exon2.Gilbert Exon 2.1	Fwd: TTGCCATGGAAACCTGTGAC Rev: GGACCAACTCCTGCTAATGC
Exon 2.2	Fwd: GCATGATCATCGGATGACCC Rev: CCTTGCCACTGATGCCATAG
Promoter 1	Fwd: CCCTTCTTGCTCTGTGTGTG Rev: TTCCCCTGCAGTTCCTACTC

Synthego ICE Analysis

Amplifying primers	Sequencing Primers
Fwd: CAACATGTCCGTTCGGTGAAG Rev: GATCTCAACTGCTGCTCTGTAAG	Fwd: GCCCACTTTCTTTGGAGTCC Rev: GCAAAAGTGAAGCCTTGCTG

2.2 Modeling and quantifying neurogenesis in phNPCs

2.2.1 Culturing phNPCs under proliferation and differentiation conditions

Cells were cultured as described before (Stein et al., 2014). Undifferentiated phNPCs were cultured in proliferation media [Neurobasal A (Invitrogen) supplemented with 10% BIT (Stem Cell Technologies), Antibiotics and Antimycotics (Gibco), GlutaMAX (Gibco), and heparin (1 µg/mL; Sigma)] with freshly added EGF, FGF2, PDGF (each at 20 ng/mL; Peprotech), and LIF (2 ng/mL; Millipore) and passaged when confluent. For differentiation, low passage (5-10) cells were plated at 2x104 cells/cm² on polyornithine/laminin coated plastic plates or acid washed coverslips, and then switched to differentiation media [Neurobasal A (Invitrogen) supplemented with B27 (Gibco), GlutaMAX (Gibco), and Antibiotics and Antimycotics (Gibco)] as well as Retinoic Acid (500 ng/mL; Sigma), Forskolin (10 µM; Sigma), BDNF (10 ng/mL; Peprotech), NT-3 (10 ng/mL; Peprotech), and KCl (10mM). Half of the media was replaced three times per week for the duration of the differentiation.

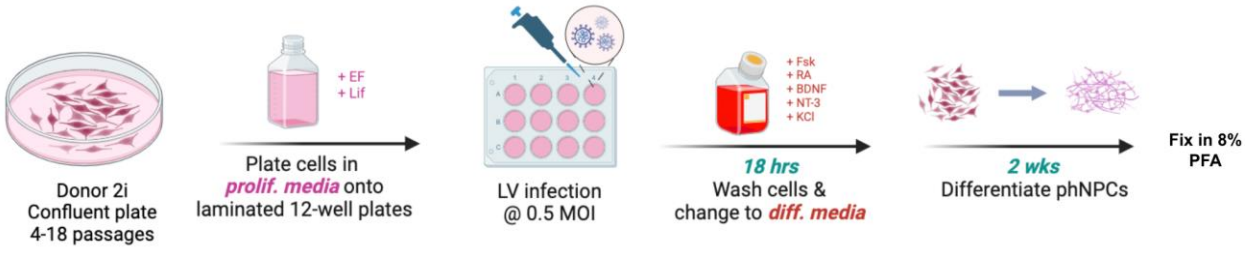

Figure 2.2: LV-infection procedure to assess ZFHX4 function in phNPC-modeled neurogenesis. 110 K cells were plated into each well of a PLO-laminin -coated 12-well plate under proliferative conditions. Cells were infected at an MOI of 0.5 < 1 hr after plating. 18 hours later, cells were washed and switched to differentiation media. Cells were cultured for 2 weeks under differentiation conditions then fixed in PFA.

2.2.2 Immunocytochemistry in phNPCs

Cells were fixed in a solution of 4% PFA and 4% sucrose, permeabilized in 0.1% Triton X-100 PBST and blocked with 10% normal donkey/goat serum in PBST. Immunostaining was performed by overnight incubation in primary antibodies diluted in 0.1% Triton X-100 PBST and 1% normal donkey serum at 4°C followed by incubation in fluorophore-conjugated secondary antibodies (Invitrogen) and staining with the DNA-binding dye 4',6-diamidino-2-phenylindole (DAPI). Primary antibodies used for ICC are listed below (Table 2.3). Images were captured by fluorescence microscopy and analyzed using ImageJ software.

Table 2.3: Primary antibodies and their experimental applications (Immunocytochemistry: ICC; Immunohistochemistry: IHC; Immunoprecipitation: IP)

Antibody	Catalogue number	Application
Ms α ZFHX4	H00079776-M11	ICC, IHC, IP
Rb α ZFHX4	HPA023837	ICC, IHC, IP
Ck α GFP	ab13970	ICC, IHC
Ms α tRFP	TA150061S	IHC
Ms α tRFP	RF5R	ICC, IHC
Rb α tRFP	AB233	ICC, IHC
Ms α Ki67	610968	ICC
Ms α TuJ1	T8660	ICC
Gp α GFAP	173 005	ICC
Rb α NESTIN	ABD69	ICC
Rb α MYT1L	25234-1-AP	IHC
Rb α NEUROD2	ab104430	ICC, IHC
Gt α SOX2	sc-17320	ICC, IHC
Ms α SATB2	ab51502	IHC, IP
Rb α SOX2	MAB3579	IP
Ms α GAPDH	MAB374	IP

2.3 Modeling and quantifying neurogenesis in OSCs

2.3.1 Preparation, LV-infection and culturing of organotypic slice culture

To prepare organotypic slice cultures from human developing cortical tissue, tissue is washed in dissection media [HBSS Ca2- Mg2- (Gibco) supplemented with HEPES (Gibco), Sodium Pyruvate (Gibco), and Antibiotics and Antimycotics (Gibco)] and then transferred to fresh, ice-cold dissection media. The composition of collection, dissection, and culturing media have been previously described (Hansen et al., 2010; Pollen et al., 2019). Tissue is sectioned into 0.5 -1 cm thick regions with sterilized instruments and cataloged. Although cortical identity can be determined by the presence of gyri in large sheet-like pieces, areal identity can only be determined in intact hemispheres.

Tissue was sectioned into 300 μm-thick sections with a vibratome (Leica Vibratome 1200S). Typically, six slices spanning the entirety of the GZ to the CP can be produced from a 2-3mm piece. Slices are placed onto 0.4 μm polytetrafluoroethylene culture inserts (Fisher PICM0RG50) and cultured at the liquid-air interface with materials and methods previously established (Figure 2.3; Hansen et al., 2010; Pollen et al., 2019). Culture plates are equilibrated in an incubator set to 37 C and 5% CO2. sgRNAs cloned into a dCas9-KRAB-P2A-GFP lentiviral vector were delivered into human neocortical organotypic slices at a concentration of 0.5MOI. 3-5uL of LV tittered at ~$1.5X10^6$ infectious units (IFU/μL) applied to the tissue (Thermo Fisher PrecisionGlide Hypodermic Needle). Micro-injection was performed within an hour of plating slices onto culture inserts and is targeted to the lower boundary of the GZ. Over the 10–14-day culturing period outlined below, OSCs were periodically replenished with OSC culture media [HBSS Ca2+ Mg2+ (Gibco) supplemented with BME (Gibco), FBS (Gibco), GlutaMax (Gibco), D+Glucose (Sigma), N-2 (Gibco) and Antibiotics and Antimycotics (Gibco)]

and live-imaged. Slices were then fixed via submersion in 4% paraformaldehyde then stored in PBS with sodium azide at 4 degrees for future processing. Disruption of cellular processes involved in neurogenesis was assessed by time lapse microscopy in cultured OSCs and immunostaining fixed OSCs for canonical markers of neural progenitors, intermediate progenitors and subtypes of excitatory neurons.

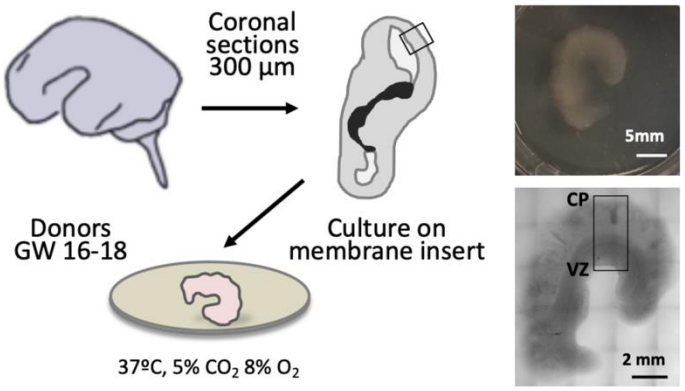

Figure 2.3: Organotypic slice culture. Left, mid-gestion cortex is sectioned into slices, plated onto membrane inserts, and cultured at the liquid-air interface. Right, slices display cortical lamination that is formed in a distinct "inside-out" pattern spanning from the innermost, progenitor rich ventricular zone to the outer cortical plate composed of mature neurons. Figure courtesy of Dr. Susanne Nichterwitz.

2.3.3 Quantifying migration in OSCs

Time Lapse imaging of GFP+ cells was performed in a Leica DM8i equipped with an environmentally controlled chamber to monitor neural progenitor proliferation, differentiation and newborn-neuron migration and positioning in specific laminae. Images across timepoints and experimental conditions were analyzed in ImageJ. First, the outline of the entire slice was manually drawn in addition to the CP/GZ boundary. Then, each LV-infected (GFP+) cell was manually selected using the Fiji Cell Counter analysis feature, which returned the raw data of the

individual Cartesian points for each labeled cell. The normalized differences of select neurons in the cortical plate and the germinal zone was computed in R Studio by measuring their distances from either the cortical plate, germinal zone, or the middle boundary separating the two regions. Distances were normalized to a value between 0-1, with 0 representing the lower GZ boundary, 1 representing the upper CP boundary, and 0.5 representing the GZ/CP boundary (Figure 2.4). These standardized measurements were used to compare relative migration within a single condition across time points, or migration within a time point across experimental conditions. Statistical significance was calculated using one-factor analysis of variance (ANOVA) and Tukey's honest significance test (HST).

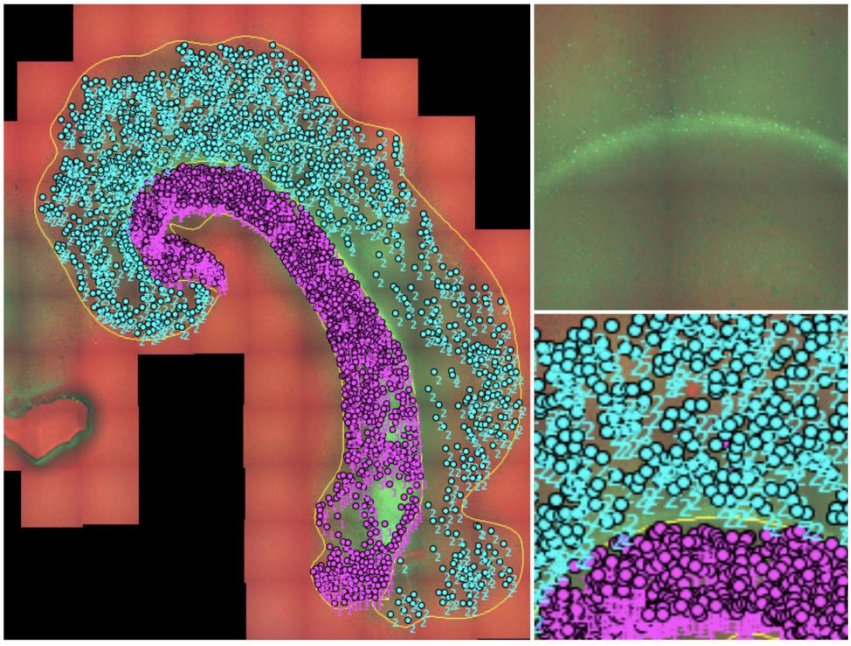

Figure 2.4: Quantifying migration in OSCs. Left, live images of OSCs taken via fluorescent microscopy are analyzed with ImageJ software. The perimeter of the tissue is drawn as well as the boundary between the GZ and the CP. All infected cells (GFP+) are manually labeled and distinguished between whether they reside in the GZ (purple labels, "1") or CP (blue labels, "2"). Right, a close-up of the GZ/CP boundary.

2.3.4 Quantifying neurogenesis in OSCs

After 10-14 days of culturing, slices are incubated in 4% PFA for 2 hours at 4C then washed with PBS. The slice is removed from the culture membrane using a paintbrush and permeabilized in 1% TritonX-100 in PBS then blocked in 10% normal donkey serum in 0.5% TritonX-100 in PBS overnight at 4C. Slices were then transferred to solution containing primary antibodies in 10% Serum in 0.5% TritonX-100 in PBS and incubated for 48-56 hours at 4C. Primary antibody solution was washed with 10% normal donkey serum in 0.1% TritonX-100 in PBS for an hour at room temperature before incubation in secondary antibody solution in PBS. Primary antibodies used for IHC OSCs are listed in Table 2.3. Slices were washed with PBS, incubated in DAPI solution (1µg/ml in PBS) for ten minutes at room temperature, then washed again with PBS. Slices were then placed in Prolong gold onto Superfrost microscope slides and covered with a coverslip. Slides were dried overnight at room temperature in the dark, then imaged by fluorescent microscopy prior to long-term storage at -20C. Images were analyzed in ImageJ to classify infected (GFP+) cells as progenitor (SOX2+ NEUROD2-), intermediate progenitor (SOX2+ NEUROD2+) or neuronal cell populations (SOX2- NEUROD2+).

References

Alerasool, N., Segal, D., Lee, H., & Taipale, M. (2020). An efficient KRAB domain for CRISPRi applications in human cells. *Nature Methods*, *17*(11), 1093–1096. https://doi.org/10.1038/s41592-020-0966-x

de la Torre-Ubieta, L., Stein, J. L., Won, H., Opland, C. K., Liang, D., Lu, D., & Geschwind, D. H. (2018). The Dynamic Landscape of Open Chromatin during Human Cortical Neurogenesis. *Cell*, *172*(1–2), 289-304.e18. https://doi.org/10.1016/j.cell.2017.12.014

Hansen, D. V., Lui, J. H., Parker, P. R. L., & Kriegstein, A. R. (2010). Neurogenic radial glia in the outer subventricular zone of human neocortex. *Nature*, *464*(7288), 554–561. https://doi.org/10.1038/nature08845

Heckl, D., Kowalczyk, M. S., Yudovich, D., Belizaire, R., Puram, R. V., McConkey, M. E., Thielke, A., Aster, J. C., Regev, A., & Ebert, B. L. (2014). Generation of mouse models of myeloid malignancy with combinatorial genetic lesions using CRISPR-Cas9 genome editing. *Nature Biotechnology*, *32*(9), 941–946. https://doi.org/10.1038/nbt.2951

Parsi, K. M., Hennessy, E., Kearns, N., & Maehr, R. (2017). Using an Inducible CRISPR-dCas9-KRAB Effector System to Dissect Transcriptional Regulation in Human Embryonic Stem Cells. *Methods in Molecular Biology (Clifton, N.J.)*, *1507*, 221–233. https://doi.org/10.1007/978-1-4939-6518-2_16

Polioudakis, D., de la Torre-Ubieta, L., Langerman, J., Elkins, A. G., Shi, X., Stein, J. L., Vuong, C. K., Nichterwitz, S., Gevorgian, M., Opland, C. K., Lu, D., Connell, W., Ruzzo, E. K., Lowe, J. K., Hadzic, T., Hinz, F. I., Sabri, S., Lowry, W. E., Gerstein, M. B., … Geschwind, D. H. (2019). A Single-Cell Transcriptomic Atlas of Human Neocortical Development during Mid-gestation. *Neuron*, *103*(5), 785-801.e8. https://doi.org/10.1016/j.neuron.2019.06.011

Pollen, A. A., Bhaduri, A., Andrews, M. G., Nowakowski, T. J., Meyerson, O. S., Mostajo-Radji, M. A., Lullo, E. D., Alvarado, B., Bedolli, M., Dougherty, M. L., Fiddes, I. T., Kronenberg, Z. N., Shuga, J., Leyrat, A. A., West, J. A., Bershteyn, M., Lowe, C. B., Pavlovic, B. J., Salama, S. R., … Kriegstein, A. R. (2019). Establishing Cerebral Organoids as Models of Human-Specific Brain Evolution. *Cell*, *176*(4), 743-756.e17. https://doi.org/10.1016/j.cell.2019.01.017

Replogle, J. M., Norman, T. M., Xu, A., Hussmann, J. A., Chen, J., Cogan, J. Z., Meer, E. J., Terry, J. M., Riordan, D. P., Srinivas, N., Fiddes, I. T., Arthur, J. G., Alvarado, L. J., Pfeiffer, K. A., Mikkelsen, T. S., Weissman, J. S., & Adamson, B. (2020). Combinatorial single-cell CRISPR screens by direct guide RNA capture and targeted sequencing. *Nature Biotechnology*, *38*(8), 954–961. https://doi.org/10.1038/s41587-020-0470-y

Stein, J. L., de la Torre-Ubieta, L., Tian, Y., Parikshak, N. N., Hernández, I. A., Marchetto, M. C., Baker, D. K., Lu, D., Hinman, C. R., Lowe, J. K., Wexler, E. M., Muotri, A. R., Gage,

F. H., Kosik, K. S., & Geschwind, D. H. (2014). A Quantitative Framework to Evaluate Modeling of Cortical Development by Neural Stem Cells. *Neuron*, *83*(1), 69–86. https://doi.org/10.1016/j.neuron.2014.05.035

Thakore, P. I., D'Ippolito, A. M., Song, L., Safi, A., Shivakumar, N. K., Kabadi, A. M., Reddy, T. E., Crawford, G. E., & Gersbach, C. A. (2015). Highly specific epigenome editing by CRISPR-Cas9 repressors for silencing of distal regulatory elements. *Nature Methods*, *12*(12), 1143–1149. https://doi.org/10.1038/nmeth.3630

Chapter 3: Results

3.1 CRISPR-mediated knockdown of ZFHX4 in phNPCs

3.1.1 Rationale and preliminary data

The role of ZFHX4 had yet to be characterized in a human corticogenesis model, which is critical to study its gene-regulatory functions and assess its role in lineage specification during cortical development. I have leveraged the fidelity and scalability of phNPCs alongside our validated approaches to modulate gene expression using CRISPR/cas9 gene editing (de la Torre-Ubieta et al., 2018) to test my hypothesis that ZFHX4 regulates the proliferation and differentiation of radial glial cells into neurons during human corticogenesis.

3.1.2 Generating loss of function indels models ZFHX4 knockdown in phNPCs

I modeled knockdown of ZFHX4 in phNPCs by generating loss of function (LOF) indels using CRISPR/cas9 mediated genome engineering. Frameshift indels are less likely to alter chromatin dynamics and generate unintentional effects as compared to gene excision. This approach is also more experimentally streamlined and avoids potential artifacts of line selection or of a specific mutation.

A literature search for previously validated sgRNAs targeting ZFHX4 returned a published genome-wide CRISPR-interference (CRISPRi) library that included and validated an sgRNA sequence that knocked down ZFHX4 expression in a human cell line (Gilbert et al., 2014). The sgRNA library was created by conducting a tiling screen to understand the parameters to optimize sgRNA design for CRISPRi-mediated knockdown and reported that sgRNAs targeted 50bp upstream to 300 bp downstream of a gene's transcription start site (TSS) facilitated strong CRISPRi activity. Additionally, sgRNA efficiency was maximized by excluding nucleotide homopolymers and restricting protospacers to18~21bp in length, while

neither sgRNA GC content nor target DNA strand directionality impacted sgRNA activity.

The published sgRNA falls within the second exon of ZFHX4's longest isoform. Fourteen ZFHX4 isoforms have been reported in human adult cortex brain tissue, with the longest isoform containing 11 exons and a predicted molecular weight of 397 kDA (GTex; https://gtexportal.org). I designed two single guide RNAs (sgRNAs) also targeting ZFHX4's second exon using the Benchling platform (https://benchling.com) maximizing both efficiency and specificity scores, and following reported guidelines (Gilbert et al., 2014). These sgRNAs target the farthest upstream exon that is shared across the most isoforms expressed in the developing human cortex, as indicated by data from my research group using novel single-cell full-length isoform sequencing (scIsoseq) technology (Figure 3.1; Patowary et al., 2023).

The three sgRNAs were then cloned into a lentiviral plasmid encoding Cas9 and RFP linked through a P2A ribosome-skipping site (Ran et al., 2013). Editing and knockdown efficiency were validated in phNPCs by DNA sequencing of the target locus and analysis by Synthego Interference of CRISPR Edits (ICEv2) assays (Conant et al., 2022). Detected indels are all predicted to generate LOF frameshift mutations and lead to nonsense-mediated RNA decay to reduce transcript levels. Indeed, knockdown at the mRNA level was assessed in infected phNPCs by qPCR in the two sgRNAs I designed, both of which robustly repressed ZFHX4 expression (Figure 3.2).

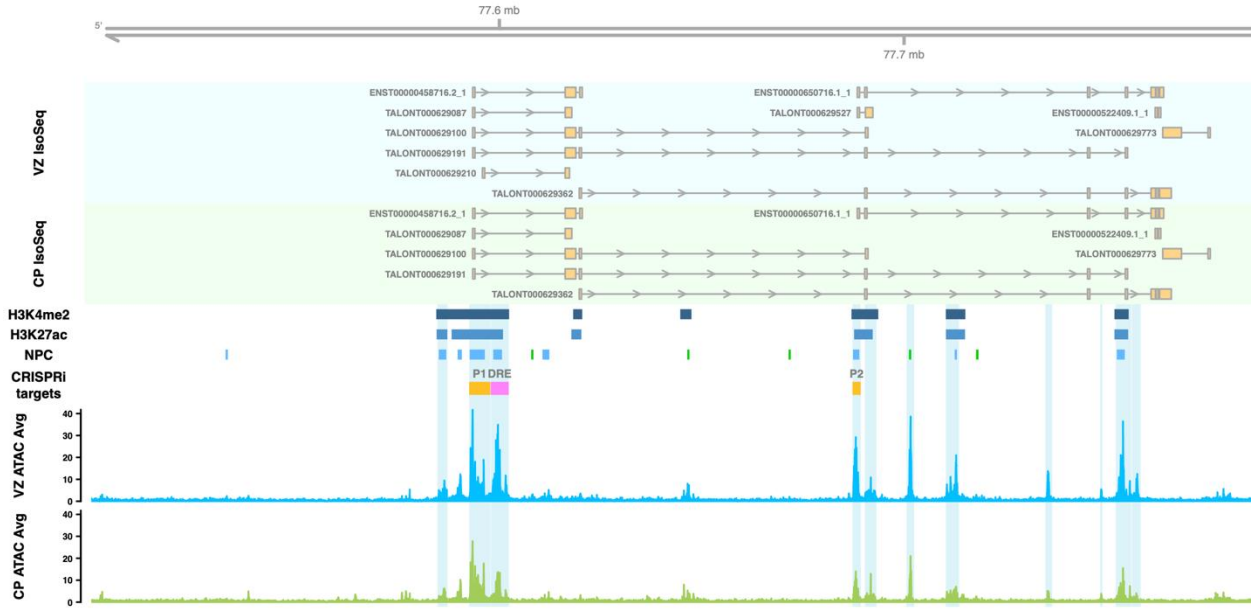

Figure 3.1: Epigenetic marks and ZFHX4 isoform expression in the CP and VZ. ZFHX4 isoforms expressed in the ventricular zone (VZ) and the CP and their genomic coordinates (top) are plotted with ChIP-seq tracks identifying active regulatory regions (H3K4me2, navy; H3K27ac, blue), and regions of chromatin accessibility in phNPCs (NPC; bulk ATAC-seq). The loci of putative ZFHX4 promoters 1 and 2 (P1, P2; orange) and differential regulatory element (DRE; pink) targeted by CRISPRi sgRNAs are annotated and overlap with ATAC-seq peaks showing regions with greater accessibility in the neocortical progenitor-enriched VZ (blue), as compared to the post-mitotic, neuron-enriched CP (green).

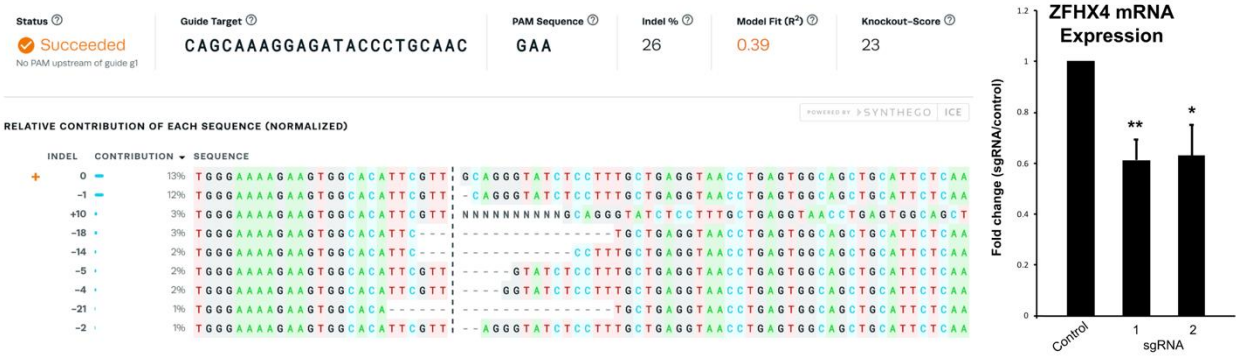

Fig 3.2: CRISPR/Cas9 mediated editing and repression of ZFHX4. Left: Synthego ICEv2 analysis of a ZFHX4-targeting CRISPR construct in HEK293T cells detecting and quantifying the sequence and proportion of the indels generated (bottom). Indel rate = 26%. Right: qPCR quantification of ZFHX4 mRNA expression in HEK293T cells edited by two different CRISPR sgRNA constructs targeting Exon 2 (ZFHX4 sgRNA Exon2.1: p = 0.003, ZFHX4 sgRNA Exon2.1: p = 0.05).

3.1.3 ZFHX4 knockdown increases neurogenesis in phNPCs after 2wks of differentiation

All three sgRNAs demonstrated similar ZFHX4 knock-down efficiency and were subsequently used to model ZFHX4 knockdown in phNPCs. For functional validation, I plated undifferentiated phNPCs on coated coverslips and infected them at 0.5 MOI, inducing differentiation through previously established methods (de la Torre-Ubieta et al., 2018; Stein et al., 2014; Won et al., 2016). After two weeks of differentiation, I fixed cells in PFA prior to performing immunocytochemistry (ICC) for validated markers or neural progenitors (GFAP) and neurons (TuJ1). Images were acquired on a fluorescent inverted microscope (Leica DMi8) then processed in Fiji, an ImageJ image processing package.

Based on our power calculations, 200-400 cells would be needed to obtain 80% power to observe effect sizes of 10-20%. In a typical differentiation experiment, ~500K cells would be fixed on a coverslip, and 15% of those cells would be infected (RFP+). Taking 20 images of a single coverslip at 10X magnification, with 10-20 infected cells per image, led to 200-400 cells being analyzed per condition per experimental replicate.

When stained for canonical cell-identity markers, differentiating phNPCs display a progressive decrease in neural stem cell markers (GFAP) with a concomitant increase in neuronal markers (TuJ1) (Stein et al., 2014). I calculated the percentage of RFP+ TuJ1+ (infected neurons) versus RFP+GFAP+ (infected progenitors) for each condition. phNPC cultures that are uninfected or have been infected with an empty control sgRNA roughly consist of a 1:5 ratio of TuJ1+ neurons to GFAP+ progenitors after two weeks of differentiation.

To assess for changes in neurogenesis upon CRISPR-mediated ZFHX4 knockdown, I compared the percent of infected cells that were TuJ1+/GFAP+ in the control condition to each of my experimental conditions. Experiments were performed in triplicates of identical but

independent experimental trials, with different plating and differentiation dates of the same line (2i), and results were analyzed by one-way analysis of variance (ANOVA) and Tukey's honest significance test (HST).

All three sgRNAs targeting ZFHX4 Exon 2 displayed a significant increase in TuJ1+ when compared to the control condition, with a concomitant decrease in GFAP+ neural progenitors (Figure 3.3, Figure 3.4). These results indicate that CRISPR/Cas9-mediated targeting of the second ZFHX4 coding exon led to increased neurogenesis in phNPCs.

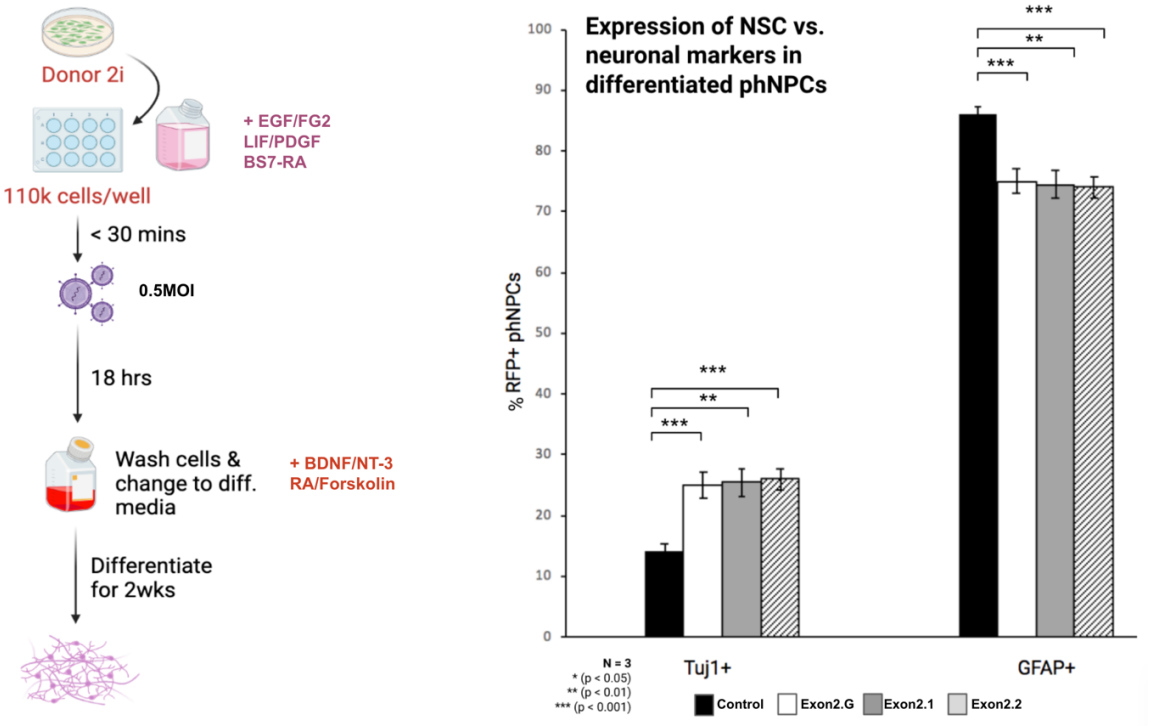

Fig 3.3: Knockdown of ZFHX4 alters neurogenesis. Left, schematic of 2wk differentiated phNPCs infected with sgRNAs targeting the second exon. Right, quantification of RFP+ TuJ1+ cells and RFP+GFAP+ cells show increased neurogenesis. Asterisks indicate $p \leq 0.05$, 0.01, 0.001 following ANOVA and Turkey's HSD. N: Control trial 1 = 13 images, 1,615 cells. Control trial 2 = 18 images, 1,715 cells. Control trial 3 = 13 images, 1,878 cells; sgRNA Exon2.G trial 1 = 10 images, 1,202 cells. sgRNA Exon2.G trial 2 = 13 images, 670 cells. sgRNA Exon2.G trial 3 = 15 images, 1,979 cells; sgRNA Exon2.1 trial 1 = 10 images, 826 cells. sgRNA Exon2.1 trial 2 = 11 images, 599 cells. sgRNA Exon2.1 trial 3 = 16 images, 2,115 cells; sgRNA Exon2.2 trial 1 = 9 images, 950 cells. sgRNA Exon2.2 trial 2 = 13 images, 449 cells. sgRNA Exon2.2 trial 3 = 15 images, 2,054 cells.

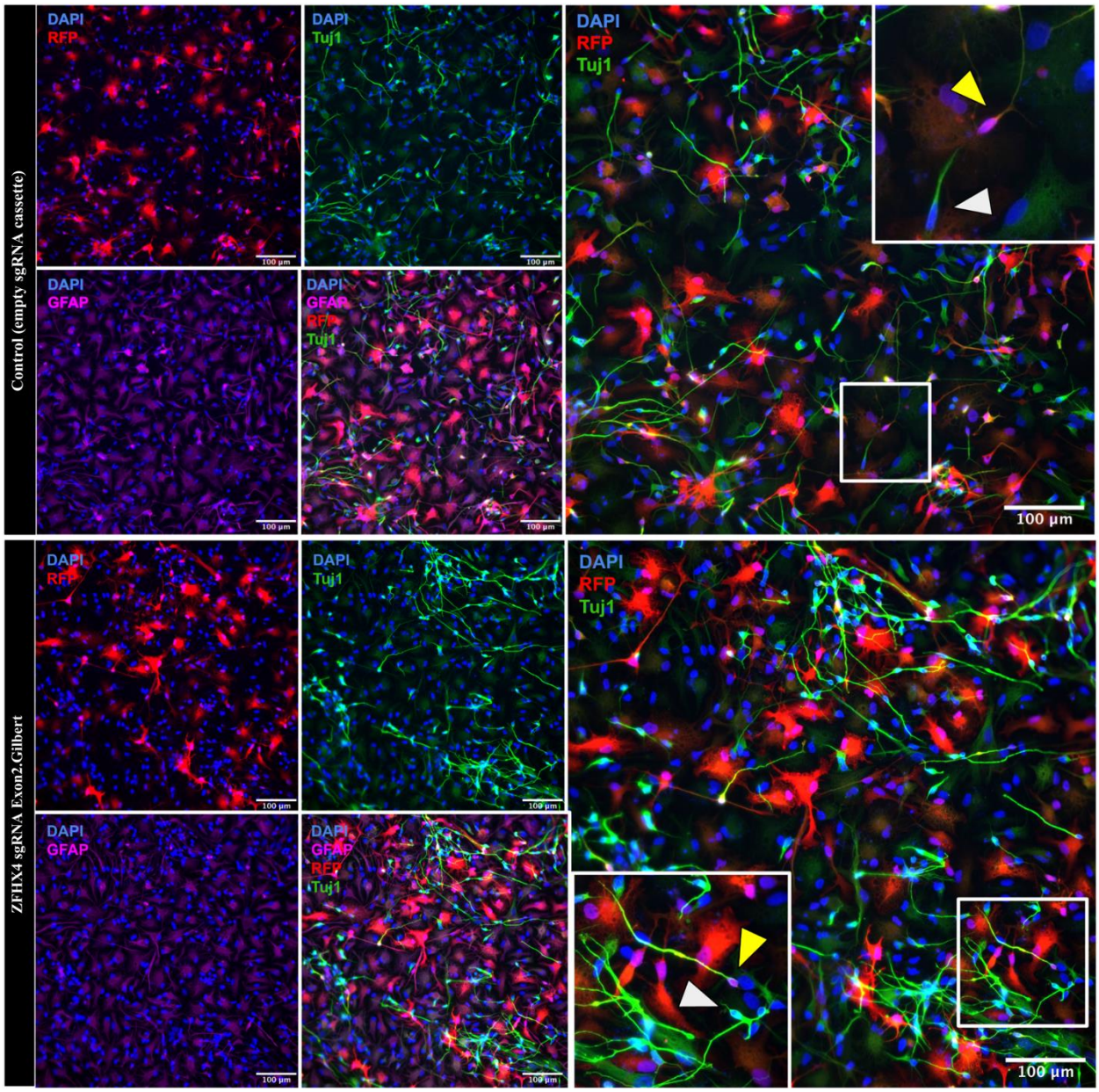

Fig 3.4: Representative ICC images of CRISPR-edited phNPCs. 2wk differentiated phNPCs infected with sgRNAs targeting the second exon show increased neurogenesis. Yellow and white arrowheads indicate infected and uninfected neurons, respectively. ICC was performed with the following primary and secondary antibody combinations: Rb α tRFP (Dk; Gt-Alexa 555); Ms α TuJ1 (Dk; Ms-Alexa 488); Gp α GFAP (Dk; Gp-Alexa 647).

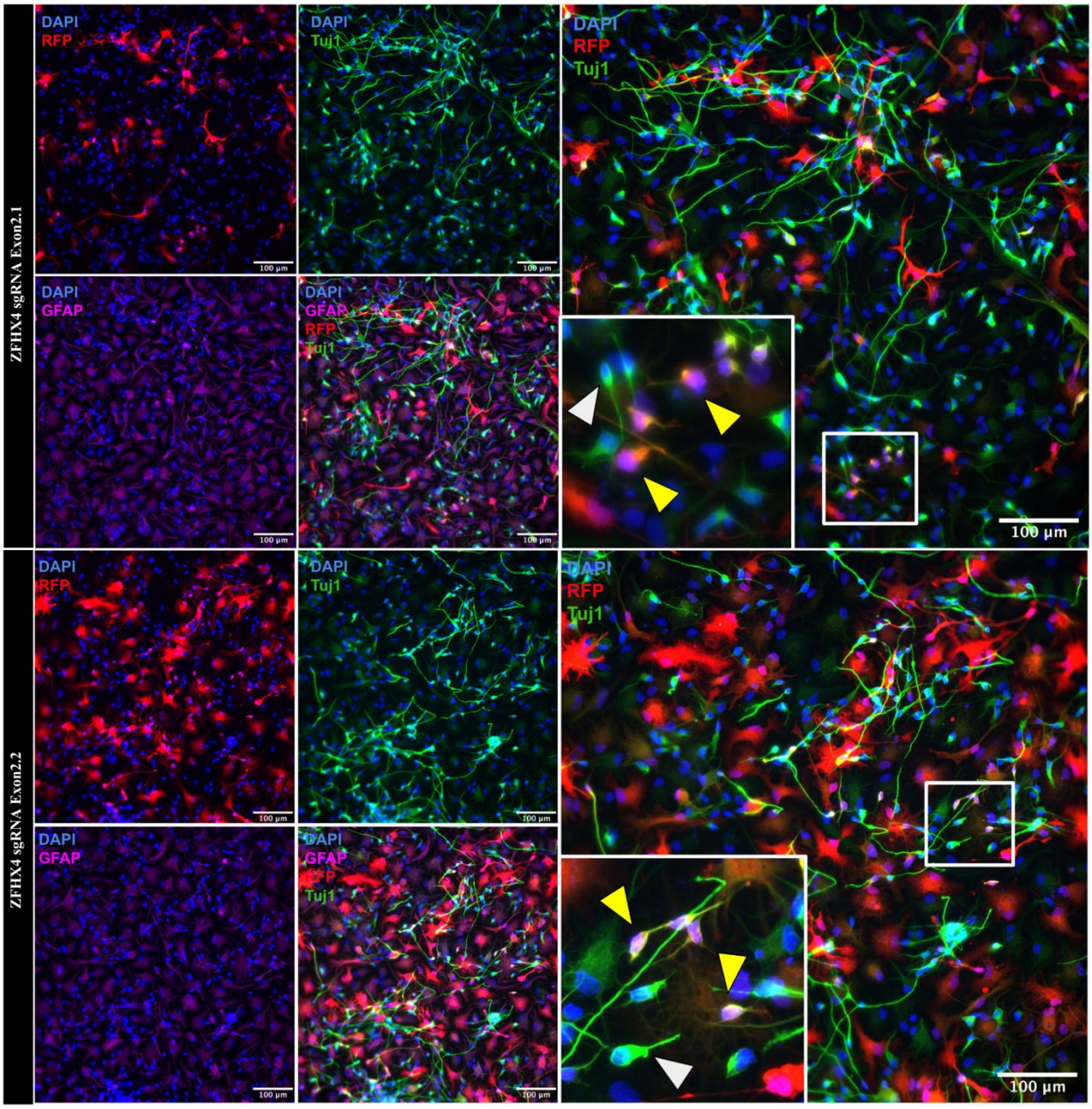

Fig 3.4: Representative ICC images of CRISPR-edited phNPCs *(cont.).* 2wk differentiated phNPCs infected with sgRNAs targeting the second exon show increased neurogenesis. Yellow and white arrowheads indicate infected and uninfected neurons, respectively. ICC was performed with the following primary and secondary antibody combinations: Rb α tRFP (Dk; Gt-Alexa 555); Ms α TuJ1 (Dk; Ms-Alexa 488); Gp α GFAP (Dk; Gp-Alexa 647).

3.1.4 Assessing for changes in cell-type composition and cell cycle dysregulation at peak neurogenesis

We have observed that knock down of ZFHX4, a TF enriched in neural progenitors, leads to premature neurogenesis in phNPCs that have undergone two weeks of differentiation. This suggests that ZFHX4 may function to maintain a proliferative progenitor state. To better understand the parameters of ZFHX4's effect on neurogenesis in phNPCs, I assessed for changes in neurogenesis upon CRISPR-mediated ZFHX4 knockdown as outlined above but extending the culturing periods from two weeks to four weeks of differentiation, after which phNPCs undergo peak neurogenesis.

I assessed for changes in neurogenesis upon CRISPR-mediated ZFHX4 knockdown, as outlined above (3.1.3: ZFHX4 knockdown increases neurogenesis in phNPCs after 2wks of neuronal differentiation) after four weeks of differentiation. Upon performing two preliminary trials, none of the three sgRNAs targeting ZFHX4 Exon 2 displayed a significant change in the proportion of TuJ1+ or GFAP+ cells when compared to the control condition (Table 3.1).

In parallel, I performed ICC at 4 weeks post-differentiation for Ki67, a validated marker of cell proliferation. Preliminary results did not indicate any disruptions to the cell cycle of proliferating progenitors upon ZFHX4 depletion, as the proportion of RFP+Ki67+ cells were similar across the control condition and the three experimental conditions. This experiment must be performed in triplicate prior to interpreting results. Additionally, this experiment should be performed in the 2-week time point, in which ZFHX4 depletion affected neurogenesis. It is possible that the effect of ZFHX4's knockdown on progenitor proliferation wanes as the cells reach peak neurogenesis, and accounts for the lack of phenotype in 4 weeks for both neurogenesis and Ki67.

Table 3.1: Knockdown of ZFHX4 does not alter neurogenesis after 4wks of differentiation. RFP+ cells were quantified and the median values (of all images per condition) are reported below.

TRIAL 1	% Tuj1+	% GFAP+	# RFP+ cells	# Images	Std. Error
Control	33.33	66.67	166.00	31.00	7.16
Exon2.Gilbert	55.56	44.44	331.00	27.00	1.23
Exon2.1	42.86	57.14	136.00	15.00	2.60
Exon2.2	37.36	62.64	190.00	18.00	1.51
TRIAL 2	% Tuj1+	% GFAP+	# RFP+ cells	# Images	Std. Error
Control	22.22	77.78	72.00	13.00	1.00
Exon2.Gilbert	36.36	63.64	292.00	25.00	1.28
Exon2.1	62.50	37.50	108.00	13.00	2.25
Exon2.2	33.33	66.67	186.00	21.00	1.39

3.2 Defining the gene regulatory mechanisms driving ZFHX4 expression in phNPCs

3.2.1 Rationale and preliminary data

In previous work, our laboratory defined gene-regulatory elements (GREs) predicted to drive gene expression programs controlling neurogenesis. I identified two distal GZ>CP GREs predicted to regulate ZFHX4 by enhancer-promoter looping using ATAC-seq and Hi-C. In preliminary studies, these GREs are also more accessible in undifferentiated phNPCs as compared to differentiated 8wk phNPCs (Liang et al., 2021) and overlap H3K27ac (active enhancer) marks from developing human cortex (Reilly & Noonan, 2016). I tested the hypothesis that ZFHX4 expression is regulated by the activity of these GREs by targeting the KRAB repressor to these loci using CRISPRi in differentiating phNPCs.

To test if these putative enhancers regulate ZFHX4 and ultimately coordinate its putative role in corticogenesis, I targeted the sequence of each candidate GRE using CRISPR interference (CRISPRi) to induce gene repression in phNPCs. CRISPRi enacts highly specific and reversible

transcriptional repression without introducing mutations to the genome (Figure 3.5). The lentiviral constructs carrying the guide sequences facilitate precise binding of a "dead" catalytically inactive Cas9 mutant (dCas9) to the target sequence. dCas9 was fused to a KRAB domain, a transcriptional repression module that binds TRIM28/KAP1 and facilitates downstream binding of the H3K9 methyltransferase SETDB1. TRIM28 and H3K9me3 sites recruits heterochromatin protein 1 (HP1), HP1 binding compacts local chromatin and sterically inhibits transcriptional machinery from accessing GREs (Thakore et al., 2015; Imbeault et al., 2017).

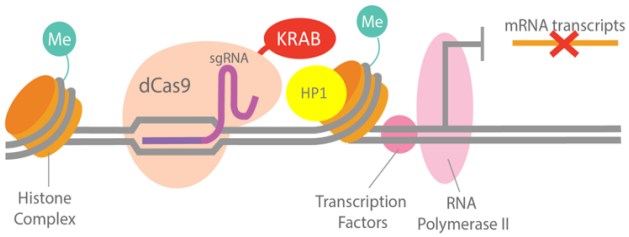

Figure 3.5: CRISPRi represses gene expression at sgRNA-targeted loci.

3.2.2 Putative GREs modulate ZFHX4 expression

I designed 1-2 sgRNAs per putative ZFHX4 GZ>CP GRE and to their target promoter GZ>CP peak (Figure 3.1) Following published guidelines for designing efficient CRISPRi guides (Pierce et al., 2021) I designed sgRNAs that targeted the center of ATAC-seq peaks where regions of open chromatin tend to be most accessible. As a negative control, I used a truncated sgRNA construct that retains the dCas9-binding hairpin but lacks the target DNA base-pairing region. The functionality of these GREs was assessed by measuring ZFHX4 expression

level by qPCR in phNPCs following 3 days of proliferation, and sgRNAs targeting the three GREs showed 25-45% knockdown (Figure 3.6).

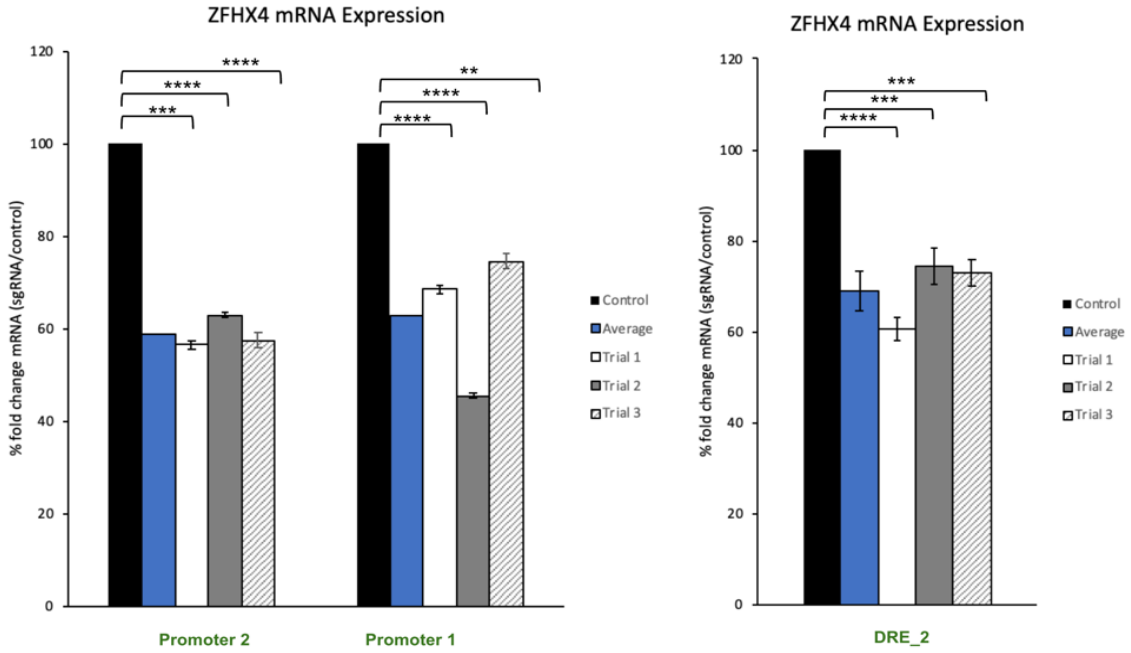

Figure 3.6: CRISPRi-mediated silencing of putative DREs decreases ZFHX4 mRNA expression. qPCR quantification of ZFHX4 mRNA expression in phNPCs performed in triplicate.

3.2.2 Modulating ZFHX4 GRE activity phenocopies CRISPR-mediated knockdown in phNPCs

Using CRISPRi, I assessed for dysregulation in neurogenesis caused by repression of candidate ZFHX4 GREs. Following the methodology used to quantify changes in differentiation and cell fate caused by CRISPR-mediated ZFHX4 knockdown, I targeted the KRAB repressor to these GREs in phNPCs, and after differentiating for two weeks, fixed and stained the cells for ICC. Upon targeting putative promoter 1, I observed a significant increase in the percent of early-born neurons (TuJ1+/GFAP-) with a concomitant decrease in neural progenitors (TuJ1-

/GFAP+) as compared to control infected cells (Figure 3.7, Figure 3.8). Similarly, modulating the activity of putative promoter 2 and a putative differential regulatory element (DRE) via CRISPRi phenocopies ZFHX4 knockdown. These results suggest that ZFHX4 operates in neural progenitors coordinating a program to regulate neurogenesis.

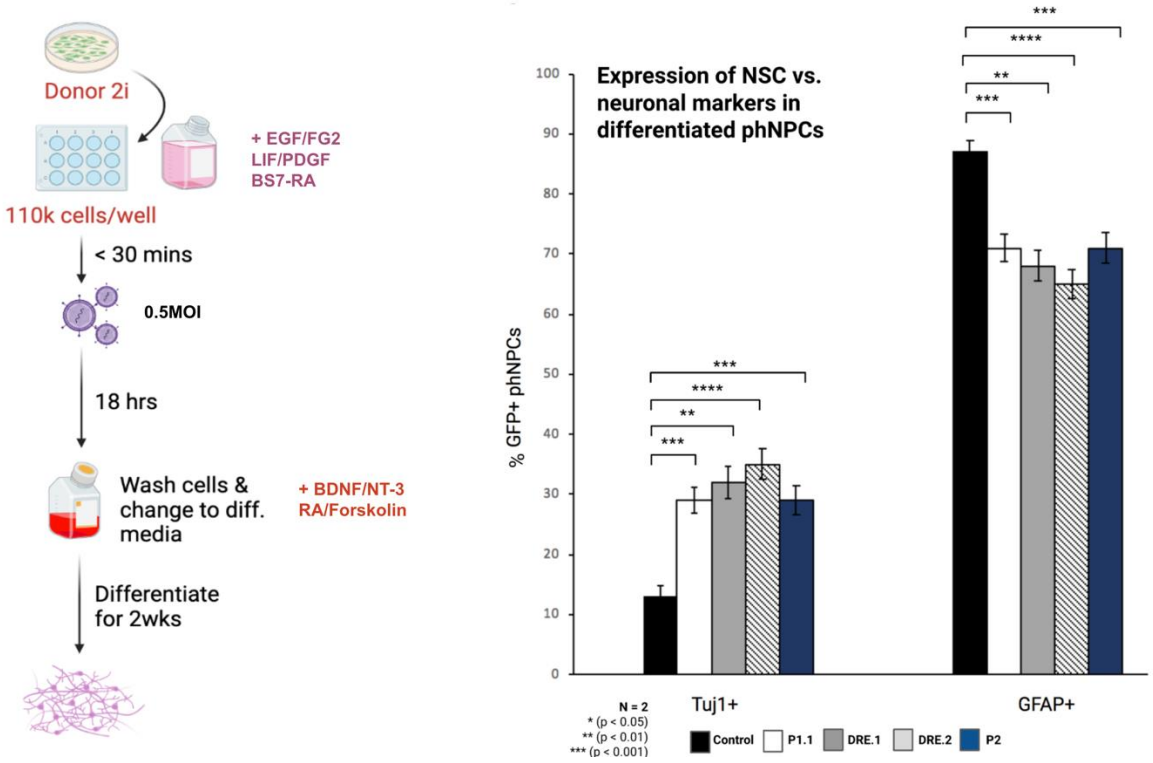

Figure 3.7: Repression of ZFHX4 GREs via CRISPRi increases neurogenesis. 2wk differentiated phNPCs transduced with sgRNAs targeting a putative DRE of ZFHX4 show increased neurogenesis. Left, schematic of 2wk differentiated phNPCs infected with sgRNAs targeting putative ZFHX4 GREs. Right, quantification of GFP+TuJ1+ cells and GFP+GFAP+ cells show increased neurogenesis. Asterisks indicate $p \leq 0.05, 0.01, 0.001, 0.0001$ following ANOVA and Turkey's HSD. N: Control Trial 1 = 14 images, 754 cells; Trial 2 = 10 images, 1,215 cells; Trial 3 = 15 images, 750 cells. ZFHX4 sgRNA DRE.1 Trial 1 = 10 images, 367 cells; Trial 2 = 10 images, 1,147 cells; Trial 3 = 14 images, 847 cells. ZFHX4 sgRNA DRE.2 Trial 1 = 10 images, 605 cells; Trial 2 = 7 images, 1,309 cells; Trial 3 = 13 images, 496 cells. ZFHX4 sgRNA promoter 2 Trial 1 = 9 images, 508 cells; Trial 2 = 19 images, 512 cells. ZFHX4 sgRNA promoter 1 Trial 1 = 9 images, 867 cells; Trial 2 = 8 images, 1,516 cells. Trial 3 = 19 images, 512 cells.

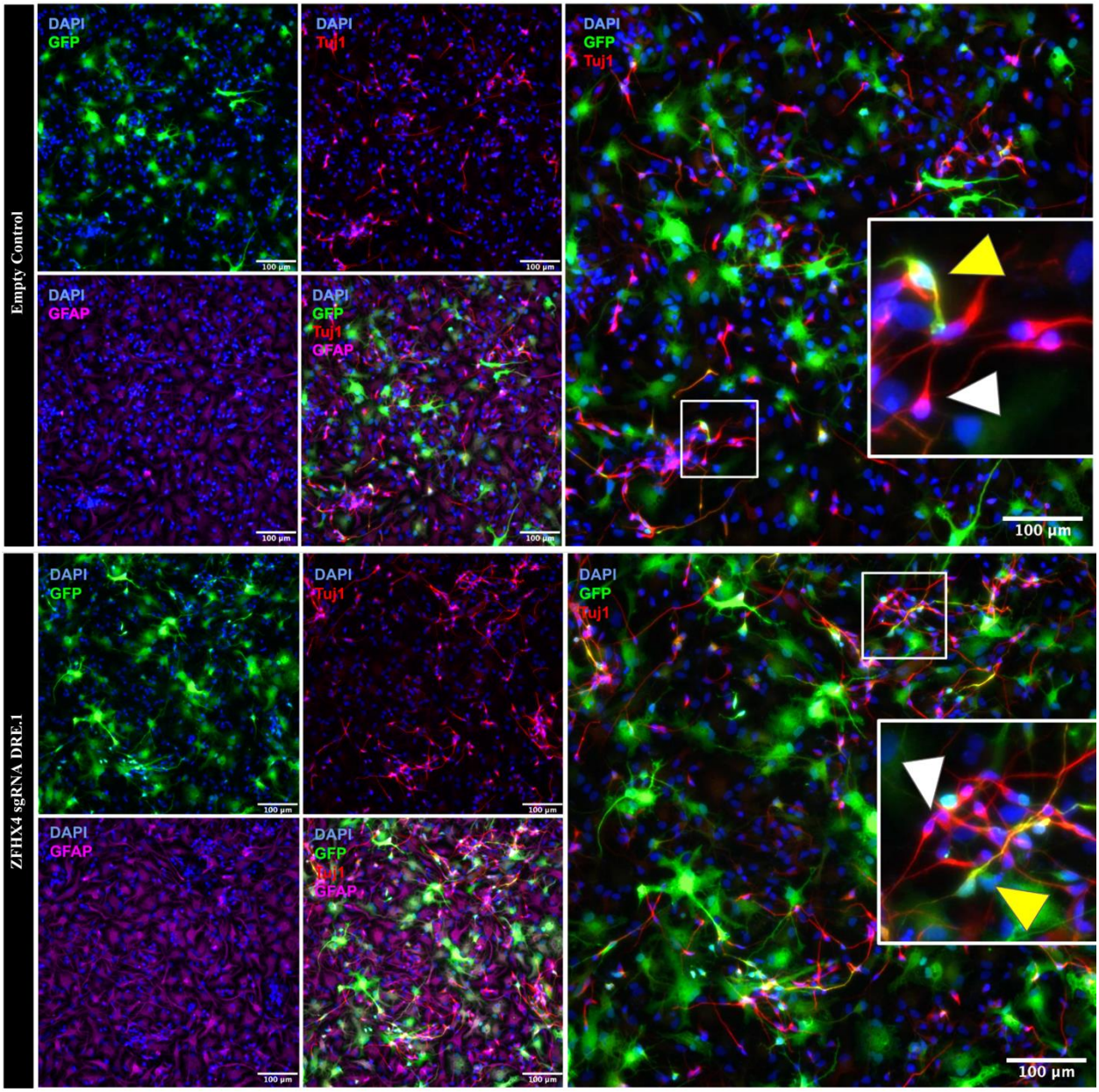

Fig 3.8: Representative ICC images of CRISPR-edited phNPCs. 2wk differentiated phNPCs transduced with sgRNAs targeting a putative DRE of ZFHX4 show increased neurogenesis. White and yellow arrowheads indicate infected and uninfected neurons, respectively. ICC was performed with the following primary and secondary antibody combinations: Ck α GFP (Dk; Gt-Alexa 488); Ms α TuJ1 (Dk; Ms-Alexa 555); Gp α GFAP (Dk; Gp-Alexa 647).

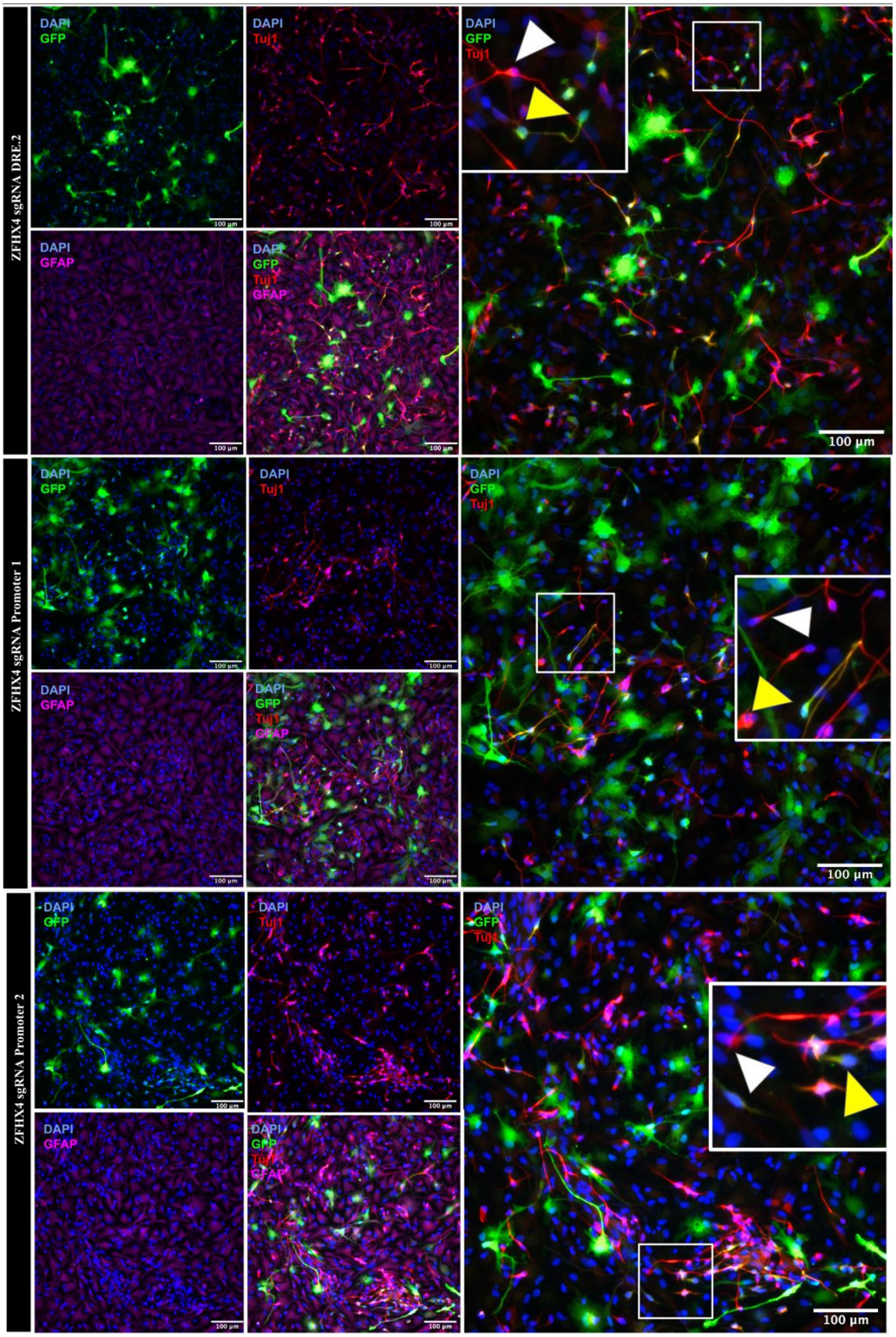

Figure 3.8: Representative ICC images of CRISPR-edited phNPC *(cont.)*.

Shortly after the completion of these experiments, a comparative study of 57 variants of the KRAB repressor was published and reported that the ZIM3 domain most efficiently represses gene expression. Specifically, the ZIM3 domain was reported to be 10-fold more potent than the Kox1 domain, which my CRISPRi experiments were conducted with (Alerasool et al., 2020). To see whether a more powerful KRAB domain would result in a greater effect size in my differentiation experiment, I cloned two sgRNAs targeting ZFHX4's annotated TSS into a lentiviral vector carrying the ZIM3 domain (Table 2.1). I conducted 2-week differentiation experiments where phNPCs were infected with lentiviral constructs carrying a control non-targeting sgRNA in addition to the two ZFHX4 TSS sgRNAs. Fixed cells were stained and analyzed via immunochemistry for canonical markers of neurons (TuJ1) and progenitors (GFAP) to assess for changes in neurogenesis. This experiment was conducted in triplicate, and CRISPRi-infected phNPCs demonstrated increased neurogenesis over control conditions (Figure 3.10, Figure 3.11). The sgRNAs targeting the ZFHX4 TSS in the ZIM3-KRAB vector demonstrated a slightly more dramatic change in cell-type composition in the 2-week differentiation experiments. However, these sgRNA targets differ from those targeting ZFHX4 GREs in the Kox1-KRAB vector, impeding direct comparison of their ability to modulate ZFHX4 activity. Overall, these observations support my hypothesis that ZFHX4 contributes to maintaining the stemness of neural progenitor cells (Figure 3.9) and demonstrates the validity of using CRISPRi methods to interrogate ZFHX4 regulation as detailed here.

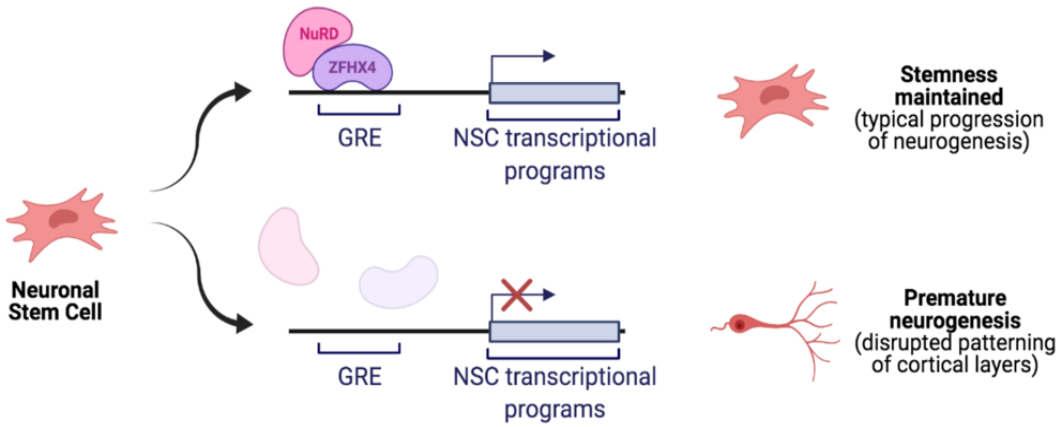

Figure 3.9: ZFHX4 is a candidate regulatory TF for human corticogenesis. ZFHX4 may contribute to coordinating human cortical neurogenesis by modulating radial glia cell proliferation and differentiation.

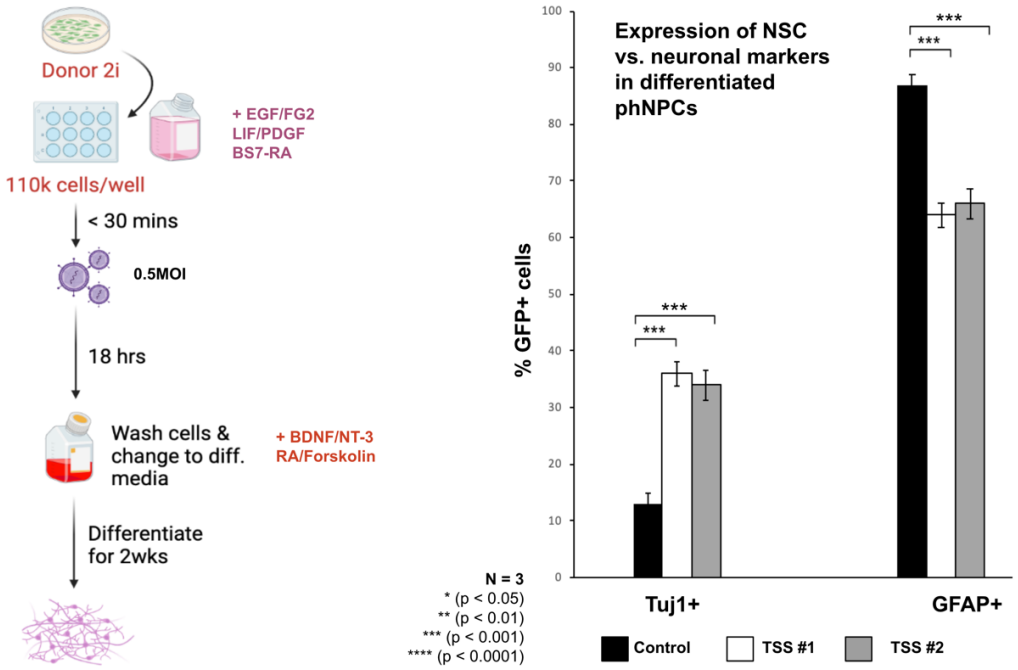

Figure 3.10: CRISPRi-targeting of ZFHX4's putative TSS increases neurogenesis.
Left, schematic of CRISPRi experiments conducted in phNPCs cultured under differentiation conditions for 2 weeks. Right, 2wk differentiated phNPCs transduced with sgRNAs targeting a putative TSS of ZFHX4 show increased neurogenesis. Asterisks indicate $p \leq 0.05$, 0.01, 0.001 following ANOVA and Turkey's HSD. N: Control trial 1 = 26 images, 251 cells. Control trial 2 = 41 images, 339 cells. Control trial 3 = 26 images, 234 cells; ZFHX4 TSS #1 = 24 images, 154 cells. Control trial 2 = 30 images, 148 cells. Control trial 3 = 25 images, 175 cells; ZFHX4 TSS #2 = 27 images, 113 cells. Control trial 2 = 43 images, 397 cells. Control trial 3 = 27 images, 108 cells.

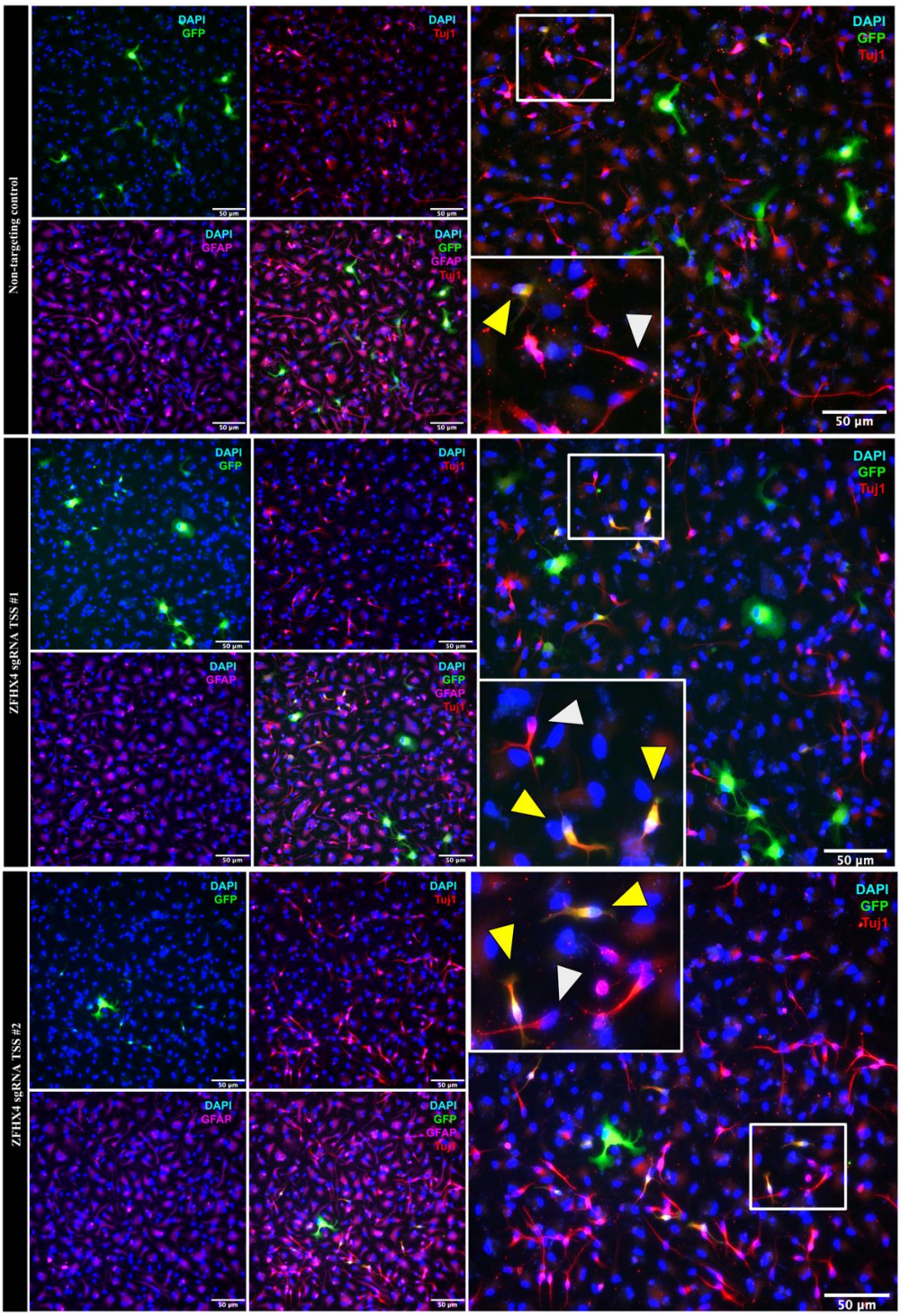

Figure 3.11: Representative ICC images of CRISPRi-edited phNPCs. 2wk differentiated phNPCs infected with sgRNAs targeting the putative transcription start site of ZFHX4 show increased neurogenesis. Yellow and white arrowheads indicate infected and uninfected neurons, respectively. ICC was performed with the following primary and secondary antibody combinations: Ck α GFP (Dk; Ck-Alexa 488); Ms α TuJ1 (Dk; Ms-Alexa 488); Gp α GFAP (Dk; Gp-Alexa 647).

3.3 Characterizing changes in neurogenesis upon ZFHX4 depletion in OSCs

3.3.1 Rationale and preliminary data

While phNPCs cultures provide the benefits of scalability and human relevance, they do not achieve functional readouts currently only possible *in vivo*, including neuronal migration and cortical layering. Here, I outline my efforts to functionally interrogate the role of ZFHX4 and its putative GREs in organotypic slice cultures (OSCs), an *in vitro* model of cortical neurogenesis.

3.3.2 Targeting ZFHX4 GREs in an *in vivo* model of neurogenesis

I have identified and validated a set of ZFHX4-associated GREs showing differential chromatin accessibility between the progenitor- enriched GZ and the post-mitotic neuron enriched CP, suggesting their participation in regulating gene expression during neurogenesis. To modulate the activity of these dynamic GREs in human cortical tissue, I will utilize my set of functionally validated sgRNAs that I have cloned into a dCas9-KRAB-P2A-GFP lentiviral vector for delivery.

I focused my analysis on samples from post conception week (PCW) 14-17 to capture a stage with substantial expansion of the outer subventricular zone, where human-enriched neural progenitors reside (Lui et al., 2011). I collected samples from three donors to conduct the experiments outlined in this section, and the details of the experimental tissue are listed below (3.2)

Directly after plating, I transduced slices by micro-injecting a concentrated titer (0.5 MOI) of lentiviral CRISPRi sgRNAs into the GZ (Figure 3.12). Since ZFHX4 is uniquely expressed in neural progenitors and enriched in ventricular radial glia, exclusively targeting the VZ for CRISPRi-ZFHX4 depletion will allow me to assess for disruption to RG-specific biological functions like neuronal migration.

Table 3.2: Donor tissue generated into OSCs. Gestation week and sample ID (donor and cortical regional) of human fetal tissue used for three trials of OSC experiments.

Trial	Donor ID & GW	CRISPR constructs	CRISPRi constructs
1	D411, R1542A (GW 17)	----	Empty sgRNA cassette
2	D408, R1530A (GW 17)	Empty control ZFHX4 Exon2.Gilbert ZFHX4 Exon2.1 ZFHX4 Exon2.2	Non-targeting control ZFHX4 Promoter 1 ZFHX4 Promoter 2
3	D409 R1536A (GW 16)	Empty control ZFHX4 Exon2.Gilbert ZFHX4 Exon2.1 ZFHX4 Exon2.2	Non-targeting control ZFHX4 Promoter 1 ZFHX4 Promoter 2 ZFHX4 DRE_1 ZFHX4 DRE_2

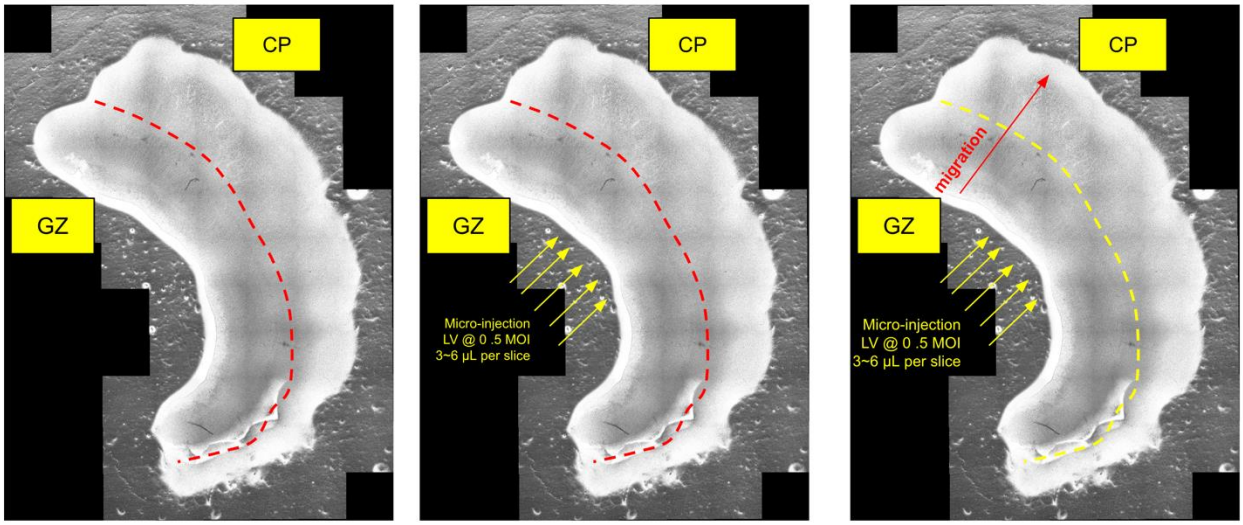

Figure 3.12: Micro-injection of LV into the GZ of OSCs. The phase image of an OSC shortly after microinjection at the GZ boundary (yellow arrows) is annotated with the boundary (red dotted line) separating the GZ and the CP.

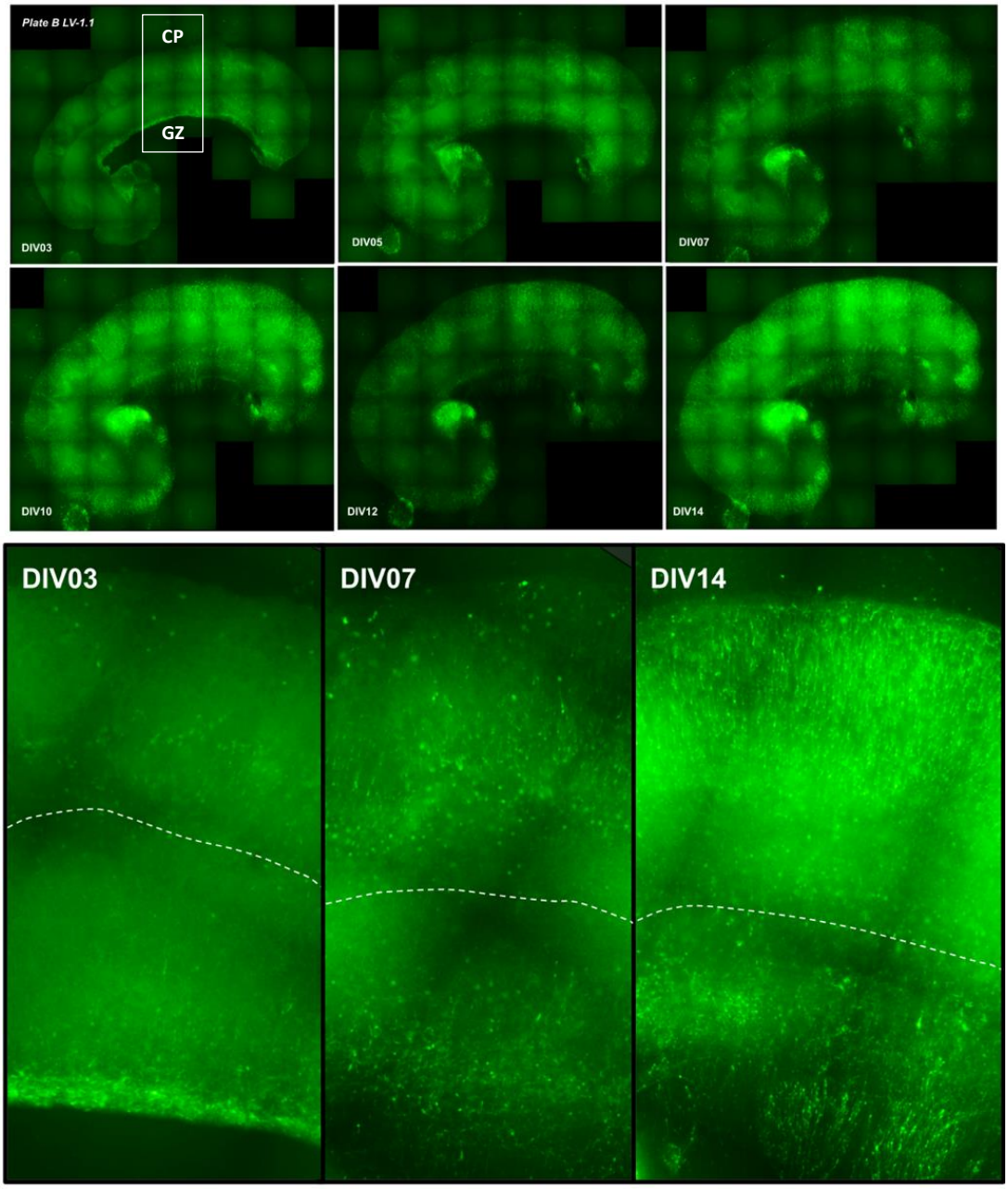

Figure 3.13: The migration of LV-infected progenitors in an OSC. Top, a single OSC was micro-injected with GFP-tagged control lentivirus (non-genome targeting sgRNA) and cultured for two weeks. Live images were taken with fluorescent microscopy on DIV (*days in vitro*) 3-14. Bottom, zoomed in images show the GZ/CP boundary, annotated with the dotted white line.

Transgene expression was observed after three days in culture, with sustained LV expression and robust physical condition of the OSCs up to 14 days in culture. Time lapse imaging of GFP+ cells were performed in a Leica DM8i equipped with an environmentally controlled chamber to monitor neural progenitor proliferation, differentiation and newborn-neuron migration and positioning in specific laminae. In a proof-of-principle experiment, time-lapse analysis demonstrated that microinjection of the VZ successfully restricts GFP-expression to the GZ of infected slices. Over the two weeks of culturing, I observed progressive migration of GFP+ cells from the VZ to the GZ (Figure 3.13). This innovation allows us target NSCs and observe the effect of CRISPRi-mediated gene silencing as they proliferate, mature, and migrate *in vivo*.

3.3.3 Assessing for changes in migration upon ZFHX4 depletion in OSCs

To assess the effect of ZFHX4's validated GREs on neuronal migration during corticogenesis, I collected and cultured organotypic human cortical slice cultures from two different donors. Slices were infected with CRISPRi sgRNAs targeting ZFHX4 GREs or a non-targeting control construct and cultured alongside an uninfected control. Trial 1 and trial 2 were cultured for 10 and 14 days, respectively. Time lapse microscopy in infected organotypic slices allowed me to measure the distance of all GFP+ cells from the GZ-boundary, the region at which cells were infected, and from where they migrate in and inside-out manner to populate and establish cortical layers (Figure 3.14, Table 3.3, Figure 3.15, Table 3.4, Figure 3.16).

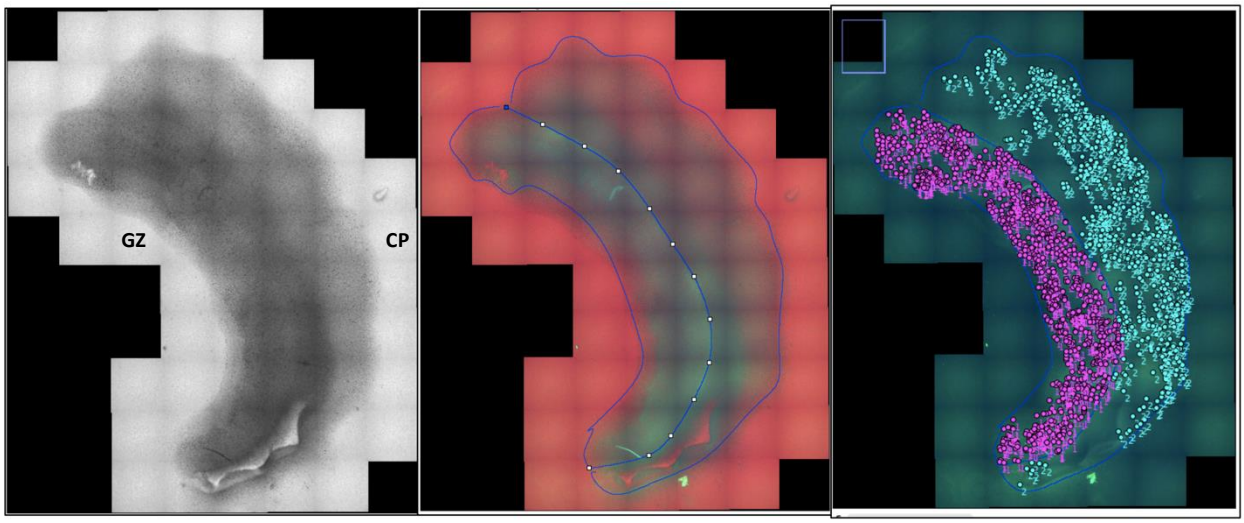

Figure 3.14: ImageJ analysis of live-imaged OSCs. Left, a phase image. Middle, the perimeter of the tissue and the GZ/CP boundary are manually drawn and superimposed onto the image. Right, GFP+ cells are quantified and categorized based on localization to the GZ (purple dots, "1") or CP (blue dots, "2").

3.3.4 Assessing for changes in cell type composition upon ZFHX4 depletion in OSCs

After 10-14 days of culturing, slices were fixed and subjected to IHC to assess alterations in neurogenesis by staining for canonical markers for neuronal cell classes. In addition to staining for GFP (channel 488) to visualize infected neurons, I tested an array of markers that, in combination, would identify and distinguish between the range of neural progenitors, intermediate progenitors and subtypes of excitatory neurons that comprise the developing neocortex (Figure 3.17). I selected for nuclear-staining markers to facilitate cell composition quantification in a tri-dimensional sample. Previously, IHC staining for SOX2 in cryopreserved neocortical slices produced robust nuclear signals in NSCs, indicating that SOX2 may be an effective NSC marker in OSCs as well. Indeed, IHC staining for SOX2 in OSCs selectively and clearly labeled NSCs in OSCs.

Table 3.3: Normalized distance of CRISPR-edited cells from the lower GZ boundary in OSCs

Trial 1; pL-CRISPR.tRFP						
DIV10	# RFP (GZ)	# RFP (CP)	# RFP (total)	Dist. (GZ)	Dist. (CP)	% CP
Ctrl	21	41	62	0.310	0.810	0.6613
Exon2.G (1)	17	19	36	0.323	0.720	0.5278
Exon2.G (2)	27	17	44	0.291	0.708	0.3864
Exon2.1	1	9	10	0.316	0.754	0.9000
Exon2.2	10	11	21	0.260	0.784	0.5238
DIV07	# RFP (GZ)	# RFP (CP)	# RFP (total)	Dist. (GZ)	Dist. (CP)	% CP
Ctrl	22	14	36	0.286	0.789	0.3889
Exon2.G (1)	18	30	48	0.296	0.750	0.6250
Exon2.G (2)	25	16	41	0.329	0.765	0.3902
Exon2.1	11	34	45	0.350	0.859	0.7556
Exon2.2	33	45	78	0.223	0.748	0.5769
DIV05	# RFP (GZ)	# RFP (CP)	# RFP (total)	Dist. (GZ)	Dist. (CP)	% CP
Ctrl	23	21	44	0.327	0.734	0.4773
Exon2.G (1)	36	36	72	0.321	0.708	0.5000
Exon2.G (2)	24	38	62	0.294	0.734	0.6129
Exon2.1	23	40	63	0.391	0.754	0.6349
Exon2.2	43	17	60	0.424	0.842	0.2833

Trial 2; pL-CRISPR.tRFP						
DIV14	# RFP (GZ)	# RFP (CP)	# RFP (total)	Dist. (GZ)	Dist. (CP)	% CP
Ctrl	13	6	19	0.1299	0.8531	0.3158
Exon2.G	1	8	9	0.2952	0.8507	0.8889
Exon2.1	8	8	16	0.4332	0.8085	0.5000
Exon2.2	10	12	22	0.2209	0.7622	0.5455
DIV08	# RFP (GZ)	# RFP (CP)	# RFP (total)	Dist. (GZ)	Dist. (CP)	% CP
Ctrl	13	7	20	0.1220	0.7488	0.3500
Exon2.G	11	5	16	0.2408	0.7274	0.3125
Exon2.1	4	2	6	0.1846	0.6773	0.3333
Exon2.2	11	2	13	0.2698	0.8812	0.1538
DIV06	# RFP (GZ)	# RFP (CP)	# RFP (total)	Dist. (GZ)	Dist. (CP)	% CP
Ctrl	23	5	28	0.1932	0.7471	0.1786
Exon2.G	9	8	17	0.3492	0.8029	0.4706
Exon2.1	8	12	20	0.2966	0.7260	0.6000
Exon2.2	9	5	14	0.2190	0.8112	0.3571

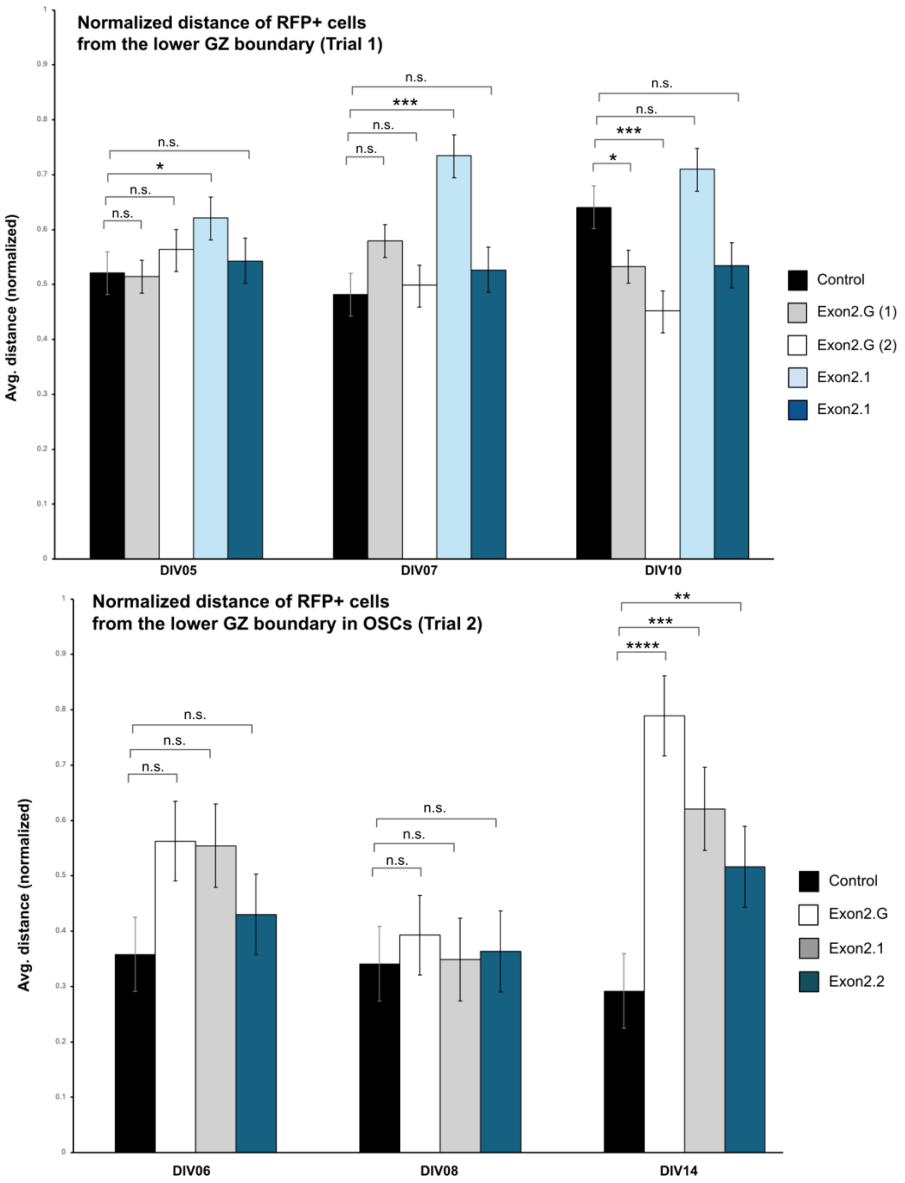

Figure 3.15: Normalized distance of CRISPR-edited cells from the lower GZ boundary in OSCs. Asterisks indicate $p \leq 0.05$, 0.01, 0.001, 0.0001 following ANOVA and Turkey's HSD. Top, Trial 1 (Donor 408, GW 17). N, 5 days *in vitro*: Control = 44 RFP+ cells; ZFHX4 sgRNA Exon2.Gilbert (1) = 72; ZFHX4 sgRNA Exon2.Gilbert (2) = 62; ZFHX4 sgRNA Exon2.1 = 63; ZFHX4 sgRNA Exon2.1 = 60. 7 days *in vitro*: Control = 36 RFP+ cells; ZFHX4 sgRNA Exon2.Gilbert (1) = 48; ZFHX4 sgRNA Exon2.Gilbert (2) = 41; ZFHX4 sgRNA Exon2.1 = 45; ZFHX4 sgRNA Exon2.1 = 78. 10 days *in vitro*: Control = 62 RFP+ cells; ZFHX4 sgRNA Exon2.Gilbert (1) = 36; ZFHX4 sgRNA Exon2.Gilbert (2) = 44; ZFHX4 sgRNA Exon2.1 = 10; ZFHX4 sgRNA Exon2.1 = 21. Bottom, Trial 2 (Donor 409, GW 16). N, 6 days *in vitro*: Control = 28 RFP+ cells; ZFHX4 sgRNA Exon2.Gilbert = 17; ZFHX4 sgRNA Exon2.1 = 20; ZFHX4 sgRNA Exon2.1 = 14. 8 days *in vitro*: Control = 20 RFP+ cells; ZFHX4 sgRNA Exon2.Gilbert = 16; ZFHX4 sgRNA Exon2.1 = 6; ZFHX4 sgRNA Exon2.1 = 13. 14 days *in vitro*: Control = 18 RFP+ cells; ZFHX4 sgRNA Exon2.Gilbert = 9; ZFHX4 sgRNA Exon2.1 = 16; ZFHX4 sgRNA Exon2.1 = 22.

Table 3.4: Normalized distance of CRISPRi-edited cells from the lower GZ boundary in OSCs

Trial 1; pLV-CRISPR-KRAB.ZIM3-GFP						
DIV10	**# GFP (GZ)**	**# GFP (CP)**	**# GFP (total)**	**Dist. (GZ)**	**Dist. (CP)**	**% CP**
Ctrl	87	33	120	0.223	0.772	0.2750
Promoter 1	47	92	139	0.385	0.828	0.6619
Promoter 2	79	45	124	0.272	0.743	0.3629
DIV07	**# GFP (GZ)**	**# GFP (CP)**	**# GFP (total)**	**Dist. (GZ)**	**Dist. (CP)**	**% CP**
Ctrl	24	43	67	0.293	0.780	0.6418
Promoter 1	40	91	131	0.347	0.821	0.6947
Promoter 2	61	38	99	0.267	0.805	0.3838
DIV05	**# GFP (GZ)**	**# GFP (CP)**	**# GFP (total)**	**Dist. (GZ)**	**Dist. (CP)**	**% CP**
Ctrl	33	14	47	0.188	0.819	0.2979
Promoter 1	65	215	280	0.428	0.784	0.7679
Promoter 2	61	14	75	0.331	0.604	0.1867
DIV03	**# GFP (GZ)**	**# GFP (CP)**	**# GFP (total)**	**Dist. (GZ)**	**Dist. (CP)**	**% CP**
Ctrl	193	71	264	0.148	0.588	0.2689
Promoter 1	174	37	211	0.204	0.839	0.1754
Promoter 2	160	53	213	0.153	0.733	0.2488

Trial 2; pLV-CRISPR-KRAB.ZIM3-GFP						
DIV14	**# GFP (GZ)**	**# GFP (CP)**	**# GFP (total)**	**Dist. (GZ)**	**Dist. (CP)**	**% CP**
Ctrl	87	99	186	0.3901	0.7662	0.5323
Promoter 1	337	358	695	0.2049	0.6185	0.5151
Promoter 2	164	184	348	0.1617	0.8204	0.5287
DRE.1	57	168	225	0.3095	0.7634	0.7467
DRE.2	293	385	678	0.3075	0.7808	0.5678
DIV08	**# GFP (GZ)**	**# GFP (CP)**	**# GFP (total)**	**Dist. (GZ)**	**Dist. (CP)**	**% CP**
Ctrl	72	80	152	0.3466	0.7783	0.5263
Promoter 1	63	64	127	0.3250	0.8020	0.5039
Promoter 2	54	73	127	0.3140	0.8250	0.5748
DRE.1	153	152	305	0.2020	0.7050	0.4984
DRE.2	298	322	620	0.2390	0.7820	0.5194
DIV06	**# GFP (GZ)**	**# GFP (CP)**	**# GFP (total)**	**Dist. (GZ)**	**Dist. (CP)**	**% CP**
Ctrl	3	4	7	0.2900	0.6720	0.5714
Promoter 1	9	24	33	0.3730	0.8250	0.7273
Promoter 2	5	5	10	0.3340	0.5370	0.5000
DRE.1	26	16	42	0.2180	0.8470	0.3810
DRE.2	52	72	124	0.2110	0.7770	0.5806

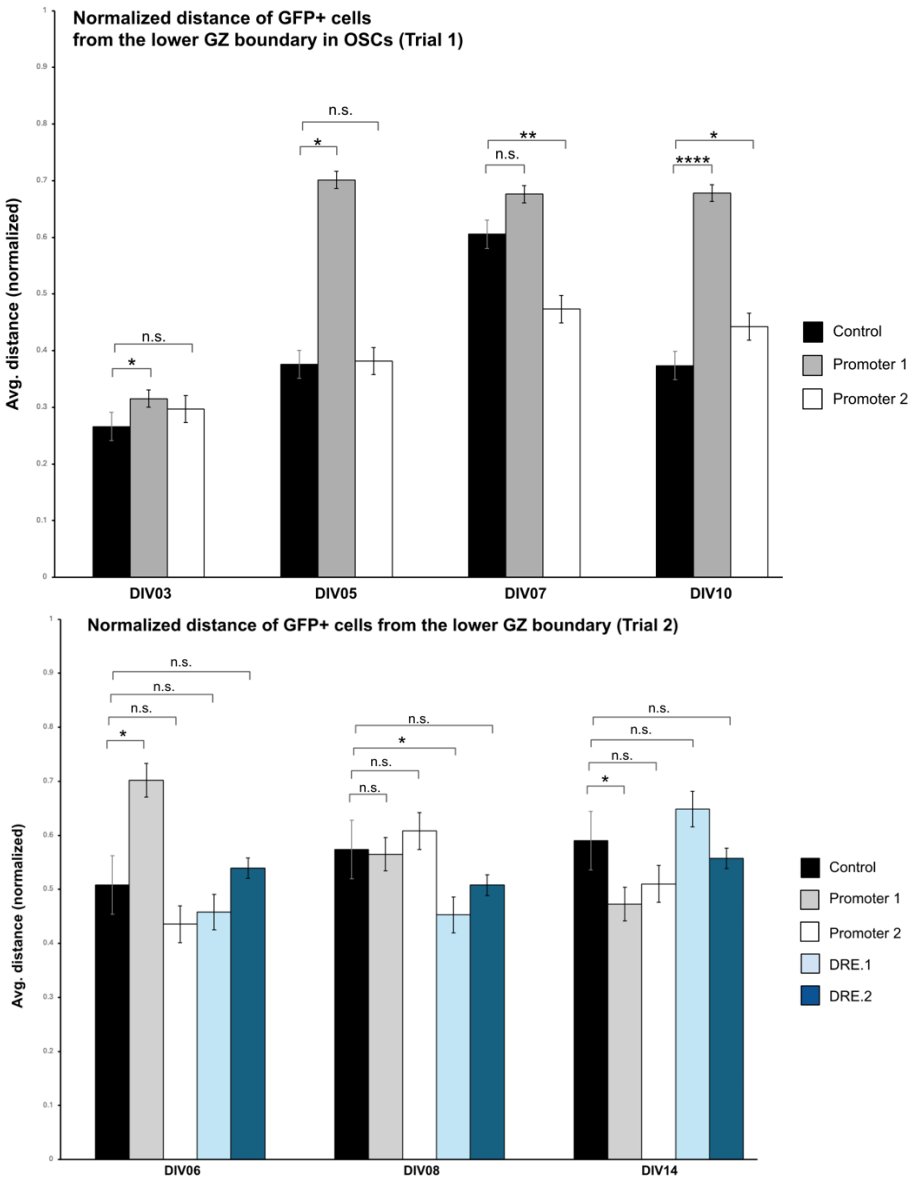

Figure 3.16: Normalized distance of CRISPR-edited cells from the lower GZ boundary in OSCs. Asterisks indicate $p \leq 0.05$, 0.01, 0.001, 0.0001 following ANOVA and Turkey's HSD. Top, Trial 1 (Donor 408, GW 17). N, 3 days *in vitro*: Control = 264 GFP+ cells; ZFHX4 sgRNA promoter 1 = 211; ZFHX4 sgRNA promoter 2 = 213. N, 5 days *in vitro*: Control = 47 GFP+ cells; ZFHX4 sgRNA promoter 1 = 280; ZFHX4 sgRNA promoter 2 = 75. N, 7 days *in vitro*: Control = 67 GFP+ cells; ZFHX4 sgRNA promoter 1 = 131; ZFHX4 sgRNA promoter 2 = 99. N, 10 days *in vitro*: Control = 120 GFP+ cells; ZFHX4 sgRNA promoter 1 = 139; ZFHX4 sgRNA promoter 2 = 124. Bottom, Trial 2 (Donor 409, GW 16). N, 6 days *in vitro*: Control = 7 GFP+ cells; ZFHX4 sgRNA promoter 1 = 33; ZFHX4 sgRNA promoter 2 = 10; ZFHX4 sgRNA DRE.1 = 42; ZFHX4 sgRNA DRE.2 = 124. 8 days *in vitro*: Control = 152 GFP+ cells; ZFHX4 sgRNA promoter 1 = 127; ZFHX4 sgRNA promoter 2 = 127; ZFHX4 sgRNA DRE.1 = 305; ZFHX4 sgRNA DRE.2 = 620. 14 days *in vitro*: Control = 186 GFP+ cells; ZFHX4 sgRNA promoter 1 = 695; ZFHX4 sgRNA promoter 2 = 348; ZFHX4 sgRNA DRE.1 = 225; ZFHX4 sgRNA DRE.2 = 678.

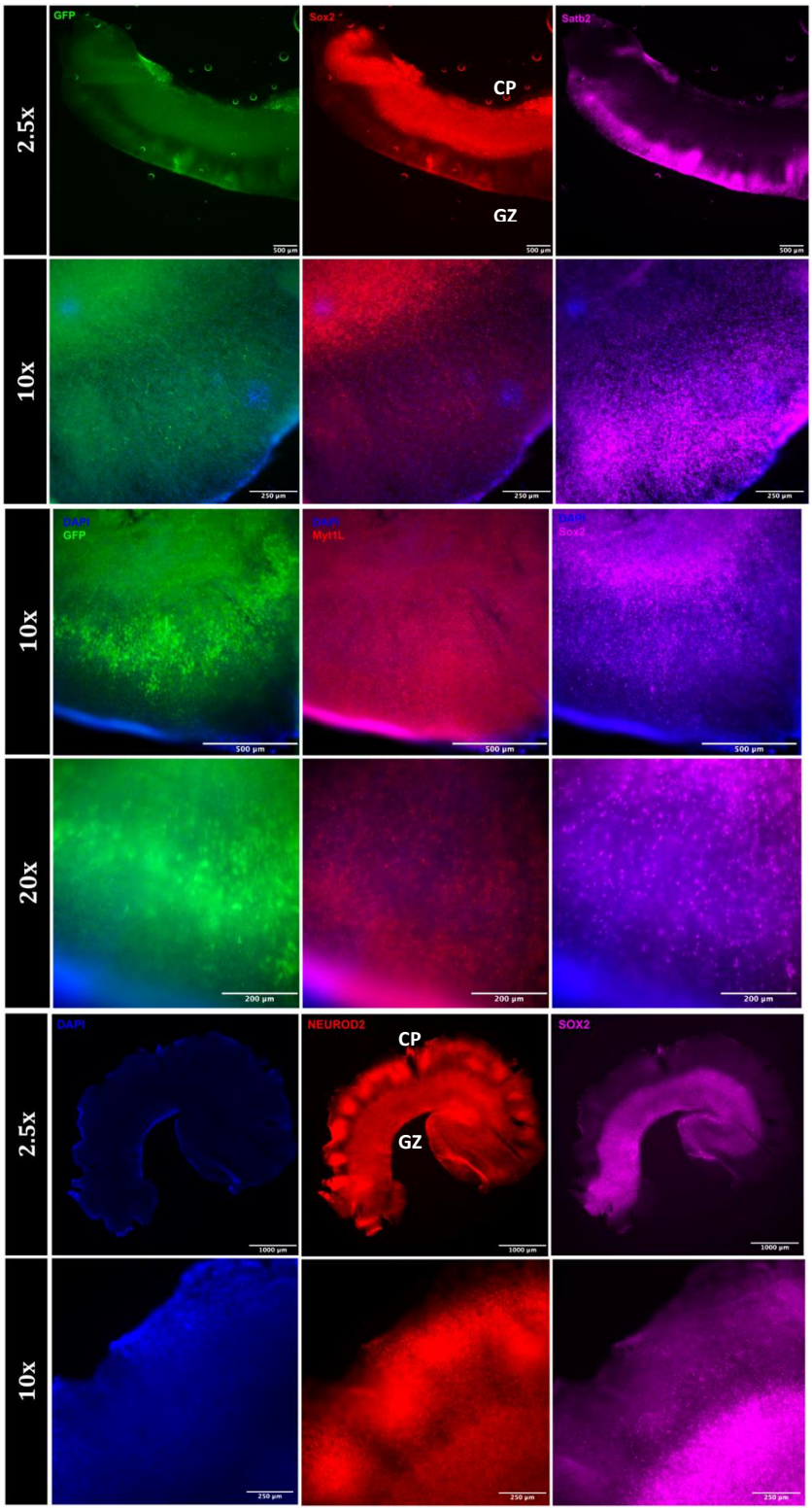

Figure 3.17: IHC images of OSCs stained for NEUROD2, SOX2, and MYT1L. Staining was performed with the following primary and secondary antibody pairings. Gt-SOX2 (Dk; Gt-647) Rb-MYT1L (Dk; Rb-555); Ck-GFP (Dk; Ck-488); Rb-NEUROD2 (Dk; Rb-555)

In combination with SOX2 staining, I tested antibodies for neuronal markers MYT1L, NEUROD2, and SATB2 (Figure 3.17). NEUROD2, but neither MYT1L nor SATB2, was co-expressed with SOX2 in some cells. I predicted that these SOX2+ NEUROD2+ cells are intermediate progenitors by utilizing the single-cell expression dataset of the developing human neocortex previously published by our research group (Figure 3.18; Polioudakis et al., 2019). To ensure that IPs could be identified and included in downstream analyses, I performed IHC on CRISPRi sgRNA-infected OSCs by collectively staining for GFP, SOX2, and NEUROD2.

I analyzed images by quantifying the number of infected progenitors (GFP+ SOX2+ NEUROD2–), infected intermediate progenitors (GFP+ SOX2+ NEUROD2+) and infected neurons (GFP+ SOX2– NEUROD2+). I compared the relative distribution of these three cell types in control conditions to CRISPRi conditions targeting ZFHX4 GREs: putative promoter 1, putative promoter 2, and the DRE. In the two preliminary trials, I did not detect any GFP+ NEUROD2+ cells in any of the control or experimental conditions (Figure 3.19). Currently, I am unable to conclusively assess for changes in neurogenesis in OSCs upon CRISPRi-mediated targeting of ZFHX4's GREs. Future attempts to do so will likely need to follow a broader survey of neuronal markers that produce robust, easily quantifiable signals in OSCs.

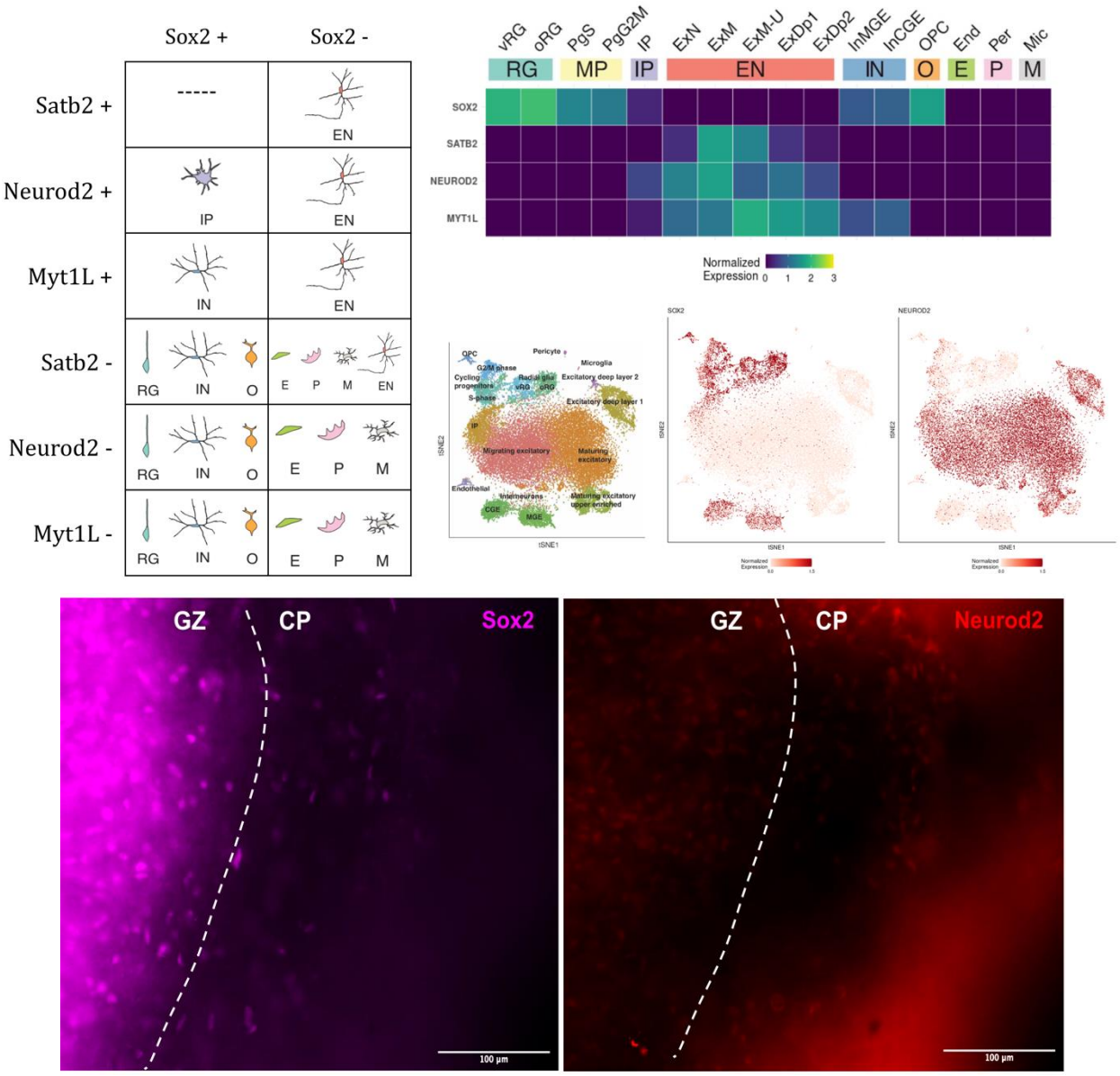

Figure 3.18: Co-expression of neural progenitor marker SOX2 with pan-neuronal markers SATB2, NEUROD2, and MYT1L. Top left, a summary of the neuronal subpopulations that can be distinguished by staining for canonical markers of cell identity. Top right, our single-cell expression dataset of the developing mid-gestation cortex shows overlapping expression of SOX2, SATB2, NEUROD2, and MYT1L across neocortical cell types. Below, a fixed OSC is stained via IHC for NSC marker expression (SOX2+), pan-neuronal marker expression (NEUROD2+), and intermediate progenitor marker expression (SOX2+ NEUROD2+). The white dotted line distinguishes between the GZ and the CP and demonstrates that both SOX2 and NEUROD2 are expressed across that GZ-CP boundary. IHC was performed with the following primary and secondary antibody combinations: Gt α SOX2 (Dk; Gt-647); Rb α NEUROD2 (Dk; Rb-555).

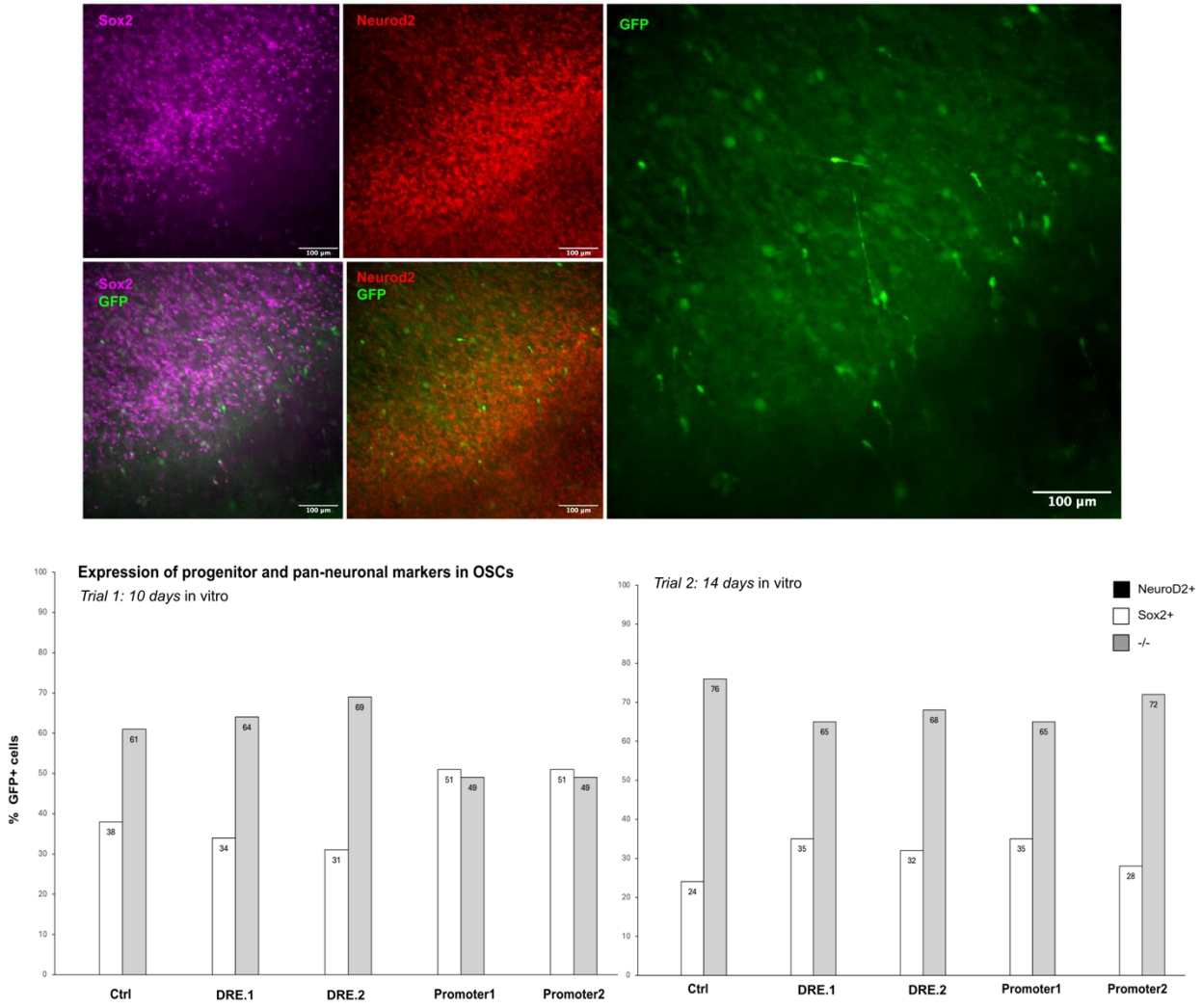

Figure 3.19: Assessing for neuronal cell-type composition in CRISPRi-infected OSCs.
LV-infected OSCs were fixed after 10 days (trial 1) or 14 days (trial 2) of culturing. Top, representative images from a trial 2 OSC slice which the GZ was micro-injected with a control construct (non-targeting sgRNA). LV-infected GFP+ cells were assessed for NSC marker expression (SOX2+), pan-neuronal marker expression (NEUROD2+), and intermediate progenitor marker expression (SOX2+ NEUROD2+). IHC was performed with the following primary and secondary antibody combinations: Gt α SOX2 (Dk; Gt-647); Ck α GFP (Dk; Ck-488); Rb α NEUROD2 (Dk; Rb-555). Bottom, quantification of N: Control trial 1 = 26 images, 251 cells. Control trial 2 = 41 images, 339 cells.

References

Alerasool, N., Segal, D., Lee, H., & Taipale, M. (2020). An efficient KRAB domain for CRISPRi applications in human cells. *Nature Methods*, *17*(11), 1093–1096. https://doi.org/10.1038/s41592-020-0966-x

Amin, N. D., & Paşca, S. P. (2018). Building Models of Brain Disorders with Three-Dimensional Organoids. *Neuron*, *100*(2), 389–405. https://doi.org/10.1016/j.neuron.2018.10.007

Chudnovsky, Y., Kim, D., Zheng, S., Whyte, W. A., Bansal, M., Bray, M.-A., Gopal, S., Theisen, M. A., Bilodeau, S., Thiru, P., Muffat, J., Yilmaz, O. H., Mitalipova, M., Woolard, K., Lee, J., Nishimura, R., Sakata, N., Fine, H. A., Carpenter, A. E., … Chheda, M. G. (2014). ZFHX4 interacts with the NuRD core member CHD4 and regulates the glioblastoma tumor initiating cell state. *Cell Reports*, *6*(2), 313–324. https://doi.org/10.1016/j.celrep.2013.12.032

Conant, D., Hsiau, T., Rossi, N., Oki, J., Maures, T., Waite, K., Yang, J., Joshi, S., Kelso, R., Holden, K., Enzmann, B. L., & Stoner, R. (2022). Inference of CRISPR Edits from Sanger Trace Data. *The CRISPR Journal*, *5*(1), 123–130. https://doi.org/10.1089/crispr.2021.0113

de la Torre-Ubieta, L., Stein, J. L., Won, H., Opland, C. K., Liang, D., Lu, D., & Geschwind, D. H. (2018). The Dynamic Landscape of Open Chromatin during Human Cortical Neurogenesis. *Cell*, *172*(1–2), 289-304.e18. https://doi.org/10.1016/j.cell.2017.12.014

Di Lullo, E., & Kriegstein, A. R. (2017). The use of brain organoids to investigate neural development and disease. *Nature Reviews. Neuroscience*, *18*(10), 573–584. https://doi.org/10.1038/nrn.2017.107

Eising, E., Carrion-Castillo, A., Vino, A., Strand, E. A., Jakielski, K. J., Scerri, T. S., Hildebrand, M. S., Webster, R., Ma, A., Mazoyer, B., Francks, C., Bahlo, M., Scheffer, I. E., Morgan, A. T., Shriberg, L. D., & Fisher, S. E. (2019). A set of regulatory genes co-expressed in embryonic human brain is implicated in disrupted speech development. *Molecular Psychiatry*, *24*(7), 1065–1078. https://doi.org/10.1038/s41380-018-0020-x

Gilbert, L. A., Horlbeck, M. A., Adamson, B., Villalta, J. E., Chen, Y., Whitehead, E. H., Guimaraes, C., Panning, B., Ploegh, H. L., Bassik, M. C., Qi, L. S., Kampmann, M., & Weissman, J. S. (2014). Genome-Scale CRISPR-Mediated Control of Gene Repression and Activation. *Cell*, *159*(3), 647–661. https://doi.org/10.1016/j.cell.2014.09.029

Happ. (2016). 8q21.11 Microdeletion in Two Patients with Syndromic Peters Anomaly. *Am J Med Genet A*, *170*(9), 2471–2475.

Imbeault, M., Helleboid, P.-Y., & Trono, D. (2017). KRAB zinc-finger proteins contribute to the evolution of gene regulatory networks. *Nature*, *543*(7646), 550–554. https://doi.org/10.1038/nature21683

Liang, D., Elwell, A. L., Aygün, N., Krupa, O., Wolter, J. M., Kyere, F. A., Lafferty, M. J., Cheek, K. E., Courtney, K. P., Yusupova, M., Garrett, M. E., Ashley-Koch, A., Crawford, G. E., Love, M. I., de la Torre-Ubieta, L., Geschwind, D. H., & Stein, J. L. (2021). Cell-type-specific effects of genetic variation on chromatin accessibility during human neuronal differentiation. *Nature Neuroscience*, *24*(7), 941–953. https://doi.org/10.1038/s41593-021-00858-w

Lui, J. H., Hansen, D. V., & Kriegstein, A. R. (2011). Development and evolution of the human neocortex. *Cell*, *146*, 18–36.

McMullan, T. W., Crolla, J. A., Gregory, S. G., Carter, N. P., Cooper, R. A., Howell, G. R., & Robinson, D. O. (2002). A candidate gene for congenital bilateral isolated ptosis identified by molecular analysis of a de novo balanced translocation. *Human Genetics*, *110*(3), 244–250. https://doi.org/10.1007/s00439-002-0679-5

Palomares, M., Delicado, A., & Mansilla, E. (2011). Characterization of a 8q21.11 microdeletion syndrome associated with intellectual disability and a recognizable phenotype. *Am J Hum Genet*, *89*, 295–301.

Patowary, A., Zhang, P., Jops, C., Vuong, C. K., Ge, X., Hou, K., Kim, M., Gong, N., Margolis, M., Vo, D., Wang, X., Liu, C., Pasaniuc, B., Li, J. J., Gandal, M. J., & Torre-Ubieta, L. de la. (2023). *Cell-type-specificity of isoform diversity in the developing human neocortex informs mechanisms of neurodevelopmental disorders* (p. 2023.03.25.534016). bioRxiv. https://doi.org/10.1101/2023.03.25.534016

Pierce, S. E., Granja, J. M., & Greenleaf, W. J. (2021). High-throughput single-cell chromatin accessibility CRISPR screens enable unbiased identification of regulatory networks in cancer. *Nature Communications*, *12*(1), 2969. https://doi.org/10.1038/s41467-021-23213-

Polioudakis, D., de la Torre-Ubieta, L., Langerman, J., Elkins, A. G., Shi, X., Stein, J. L., Vuong, C. K., Nichterwitz, S., Gevorgian, M., Opland, C. K., Lu, D., Connell, W., Ruzzo, E. K., Lowe, J. K., Hadzic, T., Hinz, F. I., Sabri, S., Lowry, W. E., Gerstein, M. B., … Geschwind, D. H. (2019). A Single-Cell Transcriptomic Atlas of Human Neocortical Development during Mid-gestation. *Neuron*, *103*(5), 785-801.e8. https://doi.org/10.1016/j.neuron.2019.06.011

Ran, F. A., Hsu, P. D., Wright, J., Agarwala, V., Scott, D. A., & Zhang, F. (2013). Genome engineering using the CRISPR-Cas9 system. *Nature Protocols*, *8*(11), 2281–2308. https://doi.org/10.1038/nprot.2013.143

Reilly, S. K., & Noonan, J. P. (2016). Evolution of Gene Regulation in Humans. *Annual Review of Genomics and Human Genetics*, *17*(Volume 17, 2016), 45–67. https://doi.org/10.1146/annurev-genom-090314-045935

Ronan, J. L., Wu, W., & Crabtree, G. R. (2013). From neural development to cognition: Unexpected roles for chromatin. *Nature Reviews Genetics*, *14*(5), 347–359. https://doi.org/10.1038/nrg3413

Stein, J. L. & de la Torre-Ubieta. (2014). A Quantitative Framework to Evaluate Modeling of Cortical Development by Neural Stem Cells. *Neuron*, *83*, 69–86.

Stein, J. L., de la Torre-Ubieta, L., Tian, Y., Parikshak, N. N., Hernández, I. A., Marchetto, M. C., Baker, D. K., Lu, D., Hinman, C. R., Lowe, J. K., Wexler, E. M., Muotri, A. R., Gage, F. H., Kosik, K. S., & Geschwind, D. H. (2014). A Quantitative Framework to Evaluate Modeling of Cortical Development by Neural Stem Cells. *Neuron*, *83*(1), 69–86. https://doi.org/10.1016/j.neuron.2014.05.035

Thakore, P. I., D'Ippolito, A. M., Song, L., Safi, A., Shivakumar, N. K., Kabadi, A. M., Reddy, T. E., Crawford, G. E., & Gersbach, C. A. (2015). Highly specific epigenome editing by CRISPR-Cas9 repressors for silencing of distal regulatory elements. *Nature Methods*, *12*(12), 1143–1149. https://doi.org/10.1038/nmeth.3630

Watanabe, M., Buth, J. E., Vishlaghi, N., de la Torre-Ubieta, L., Taxidis, J., Khakh, B. S., Coppola, G., Pearson, C. A., Yamauchi, K., Gong, D., Dai, X., Damoiseaux, R., Aliyari, R., Liebscher, S., Schenke-Layland, K., Caneda, C., Huang, E. J., Zhang, Y., Cheng, G., … Novitch, B. G. (2017). Self-Organized Cerebral Organoids with Human-Specific Features Predict Effective Drugs to Combat Zika Virus Infection. *Cell Reports*, *21*(2), 517–532. https://doi.org/10.1016/j.celrep.2017.09.047

Chapter 4: Discussion

4.1 Characterizing the role of ZFHX4 in human corticogenesis *in vitro*: Outstanding questions

Tight control of neural progenitor proliferation and differentiation regulates cortical volume, thickness, and cellular diversity. To characterize the role of novel radial glial-enriched transcription factor (TF) ZFHX4 in human cortical neurogenesis, I introduced frameshift mutations in ZFHX4 in primary human neural progenitor cells (phNPCs) using CRISPR/Cas-9 genome editing. Upon assessing for changes in cellular morphology and cell fate by immunocytochemistry (ICC) with canonical cell markers, I report that knocking down ZFHX4 in neural progenitors leads to premature neurogenesis (*3.1.3 ZFHX4 knockdown increases neurogenesis in phNPCs after 2wks of neuronal differentiation*).

To define the gene regulatory mechanisms driving ZFHX4 expression in neural progenitors, I first validated the ability of putative gene regulatory elements (GREs) to modulate ZFHX4 expression (*3.2.2 Modulating ZFHX4 GRE activity phenocopies CRISPR-mediated knockdown in phNPCs*). Through chromatin accessibility and conformation analyses, I identified three GREs with differential activity in the progenitor-rich germinal zone (GZ) versus the neuron-rich cortical pate (CP) predicted to regulate ZFHX4 expression. Modulating the activity of these GREs via CRISPR-interference (CRISPRi) phenocopies ZFHX4 knockdown. These results suggest that ZFHX4 expression is restricted to neural progenitors by *cis*-regulatory modulation by these GREs, and that this regulatory relationship contributes to human corticogenesis.

4.1.1 Controlling for line-specific artifacts, sex and genetic background

A common issue with the use of stem cell lines is that they have limitations with respect to their ability to accurately recapitulate *in vivo* brain development or that the observed effects are line specific. I have mitigated these risks by using phNPCs, an extensively characterized model that robustly recapitulates neurogenesis and early cortical development up to mid-gestation time points (Stein et al., 2014). In addition, the phNPC line I have used has been screened for the absence of CNVs known to affect neurodevelopment. However, experimental assessment of CRISPR(i)-mediated ZFHX4 perturbations should be carried out in an additional, independent line to avoid line specific effects attributed to genetic background or other factors.

4.1.2 Monitoring for changes in proliferation in phNPCs upon ZFHX4 depletion

My results indicate that the effect of ZFHX4 on modulating neurogenesis in phNPCs peaks in the early stages of neurogenesis (2 weeks of differentiation) and then wanes by peak neurogenesis (4 weeks of differentiation). Indeed, a preliminary experiment assessing for changes in progenitor proliferation upon CRISPR-mediated ZFHX4 depletion reported no significant change in the proportion of mitotic (Ki67+) cells in control vs. knockdown condition (*3.1.4 Assessing for changes in neurogenesis and cell cycle dysregulation at peak neurogenesis*). To see whether progenitor proliferation remains unchanged at the time point at which both CRISPR- and CRISPRi-mediated ZFHX4 depletion led to premature neurogenesis, ICC experiments quantifying Ki67 expression should be performed in phNPCs 2 weeks after inducing differentiation. Alternatively, bromodeoxyuridine (BrdU) pulsing experiments, which label dividing cells in a temporally specific fashion (Taupin, 2007), can be performed to determine the direct progeny of dividing progenitors at multiple time points to characterize proliferation dynamics in phNPCs.

4.2 Functional interrogation of GREs in an *in vivo* model of human corticogenesis

Genetic variants that underlie risk for neuropsychiatric disease, as well as human-specific variants, have been identified mainly within non-coding genomic regions that are thought to coordinate gene expression patterns (Ward & Kellis, 2012). Despite the richness of this work, the missing link to advance functional interpretation of epigenomic annotations relies in functionally connecting them to discrete neurodevelopmental processes. Efforts to close existing gaps in our understanding of the cellular identities, lineage relationships, and gene regulatory mechanisms that drive corticogenesis have been hindered by limited human-relevant experimental models. The cell-type diversity and layered architecture of the human neocortex are challenging to recapitulate with two-dimensional models, even in well-characterized, genetically, and experimentally accessible ones like phNPCs.

To functionally characterize GREs in an *in vivo* model of neurogenesis, I leveraged organotypic cortical slice cultures (OSCs), a tri-dimensional environment that preserves the laminar architecture of the developing human cortex. In this dissertation, I have described my efforts to interrogate the role of developmentally dynamic transcription factor ZFHX4 and its putative GREs in OSCs using CRISPR/cas9 genomic engineering technology (*3.3.2 Targeting ZFHX4 GREs in an in vivo model of neurogenesis*). These experiments should progress our understanding of the regulatory mechanisms underlying the diversity of neural progenitors and lineage relationships to postmitotic derivatives, which remain largely unknown in the human brain.

Such functional annotations are challenging because of the limited capacity for experimental manipulation in OSCs and the laborious, low-throughput nature of existing methodology. I therefore conducted initial evaluations of this system with the ZFHX4 GREs that

I had previously characterized in phNPCs (*3.2.2 Modulating ZFHX4 GRE activity phenocopies CRISPR-mediated knockdown*). My preliminary experiments show that I can successfully micro-inject the GZ with LV vectors carrying CRISPRi sgRNAs to target NSCs that allow us to measure changes in neuronal migration. However, my efforts to measure changes in cell type composition via IHC were inconclusive (*3.3.4 Assessing for changes in cell type composition upon ZFHX4 depletion in OSCs*). Targeting a well-characterized TF like EOMES, which regulates cortical neuron production and cortical thickness via effects on progenitor proliferation (de la Torre-Ubieta et al., 2018), would help validate our OSC-based experimental model.

4.3 Characterizing the role of ZFHX4 in human corticogenesis: Future directions

4.3.1 Assessing for genome-wide transcriptional changes upon ZFHX4 KD

To determine whether ZFHX4 depletion alters neurogenesis and cell fate specification, I have begun comprehensive molecular phenotyping via 10X genomics single-cell RNA-sequencing (scRNA-seq; Figure 4.1). To prepare 10X libraries, I infected proliferating phNPCs with at a low titer (0.5 MOI) to ensure single sgRNA delivery per cell. phNPCs were independently infected and cultured with each of the three CRISPR/Cas9 sgRNAs targeting ZFHX4 exon 2, as well as the control vector containing no targeting sgRNA. Shortly after plating and infecting phNPCs (18 hours), I induced differentiation and cultured cells for 4 weeks, a time point where we observe peak neural progenitor diversity (Stein et al., 2014). Cells were harvested via papain digestion, sorted via FACS to obtain a pure population of infected cells.

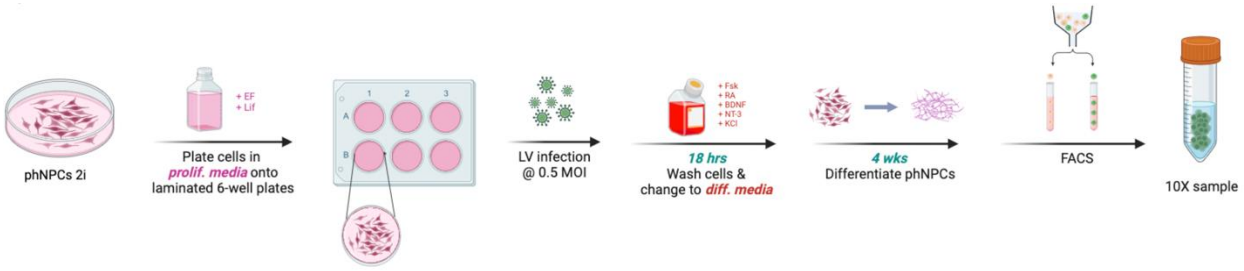

Figure 4.1: Preparing 10X genomics samples. phNPCs expressing CRISPR(i) sgRNAs were harvested at four weeks post differentiation to allow for transgene expression in both progenitors and differentiated neurons. To obtain sufficient power, a minimum target of 500,000 cells were harvested, isolated using fluorescence activated cell sorting (FACS) and subjected to scRNA-seq. We have previously optimized the methodology for isolation and sorting of infected phNPCs via FACS, obtaining millions of viable cells suitable for genomic analyses. Once generated, scRNAseq data will be harmonized with our previously defined catalog of mid-gestation human neocortical cells using the Seurat package and canonical correspondence analysis (CCA) to integrate biologically overlapping datasets with different technical covariates.

Based on previous scRNAseq (de la Torre-Ubieta et al., 2018), I have determined that a minimum of 500 nuclei at 50,000 reads/nuclei are needed to identify robust stable clusters. 5,000 differentiated cells per perturbation/time point need to be profiled to sufficiently cover the ten distinct cell types/states produced by cortical neural progenitors. This will provide stable expression signatures for the top 4000 expressed genes in that cluster (Polioudakis et al., 2019) and produce unbiased, sensitive, reliable, and representative readouts of the changes that occur in radial glial cells and their progeny over differentiation. FACS readouts indicated sufficient capture of infected cells for all four CRISPR/Cas9 constructs.

After library preparation, samples were subjected to droplet-based scRNA-seq using the10x genomics pipeline. Once the sequencing data is returned, single-cell transcriptomes will be clustered using the Seurat pipeline (Butler et al., 2018) and cluster identity will be defined using canonical markers and leveraging our single-cell gene expression atlas (de la Torre-Ubieta et al., 2018) to identify changes in either the distribution of radial glia progeny or differences in

gene expression in similar cell types. This unbiased genomic approach will allow us to identify the transcriptional programs and changes in cell fate transitions caused by ZFHX4 depletion.

I have identified and validated three ZFHX4 GREs that modulate ZFHX4 activity, and the disruption of which leads to cell fate dysregulation as assessed by ICC profiling (*3.2 Defining the gene regulatory mechanisms driving ZFHX4 expression in neural progenitors*). To further assess for molecular and cell fate dysregulation, I have prepared a CRISPRi library with a sgRNA capture tag enabling simultaneous reading of transcriptome and sgRNA at the single-cell level. The sgRNAs in this library will target the three putative GREs, a putative ZFHX4 TSS, and include two non-targeting control sgRNAs (Table 4.1). This will help reveal the extent to which ZFHX4 is transcriptionally regulated in neural progenitors and how its putative GREs influence corticogenesis.

Table 4.1: CRISPR and CRISPRi scRNA-seq libraries prepared for 10X genomics

LV vector	Control sgRNAs	ZFHX4 sgRNAs	Library assembly
pL-CRISPR.EFS.tRFP	Empty cassette	Exon2.Gilbert Exon 2.1 Exon 2.2	Individual
pLV hU6-sgRNA.CapSeq hUbC-dCas9-KRAB.ZIM3-T2a-GFP	Non-targeting sequence (1) Non-targeting sequence (2)	Promoter 1 Promoter 2 DRE_1 DRE_2 TSS1 TSS2	Pooled

4.3.2 Biochemical characterization of ZFHX4

Transcription factors regulate gene expression by associating with co-activating or co-repressive complexes with chromatin remodeling activity, and these interactions have been shown to regulate cortical neurogenesis (de la Torre-Ubieta & Bonni, 2008; Hoffmann & Spengler, 2019; Ronan et al., 2013; Sokpor et al., 2017). Previous studies suggest ZFHX4 may operate via the NuRD complex member CHD4 to regulate neurogenesis. ZFHX4 was reported to

interact with the NuRD complex member CHD4 in glioblastoma cell lines (Chudnovsky et al., 2014), supporting a mechanism where ZFHX4 may direct corticogenesis by aiding targeting of this chromatin remodeling complex to specific loci, rather than directly promoting trans-activation. The decreased proliferation of neural progenitors and microcephaly reported in CHD4-/- mice (Nitarska, 2016) is consistent with my observations of increased neurogenesis with loss of ZFHX4 and suggests a functional interaction.

To test this hypothesis, I have attempted to target ZFHX4 for co-immunoprecipitation (Co-IP) in human embryonic cortical tissue. An often-limiting factor of antibody-based immunoprecipitation is the varying quality of antibodies for different protein targets and the abundance of the target. I have mitigated this by using an IP-validated antibody for ZFHX4 (Chudnovsky et al., 2014) in addition to a separate commercially available ZFHX4 antibody.

Both antibodies target the second exon and are predicted to bind to the majority of ZFHX4 isoforms found in our preliminary IsoSeq studies (*3.1.2 Generating loss of function indels models ZFHX4 knockdown in phNPCs*). I have used both antibodies in a variety of immunostaining applications which I have optimized, including immunocytochemistry in phNPCs, immunohistochemistry of fixed organotypic slice cultures, and immunohistochemistry of fetal cryosections, all of which have yielded negative results. Preliminary immunoblotting attempts in lysed fetal tissue and lysed cell culture have been unsuccessful as well.

In lieu of antibody-based immunoprecipitation, a FLAG-tagged version of ZFHX4 can be exogenously expressed in phNPCs and immunoprecipitated by targeting the affinity tag. In addition, development of proximity-dependent biotin labeling methods such as APEX has advanced purification of proteins and their interactors without the need for antibodies (Chen & Perrimon, 2017). Briefly, an engineered ascorbate peroxidase (APEX), is fused to the protein of

interest, and cells expressing the fusion protein are incubated with the membrane-permeable biotin-phenol substrate. Upon activation with peroxidase, APEX catalyzes the addition of biotin to nearby proteins, and the reaction is quenched with sodium azide. The resulting biotinylated proteins can then be purified using streptavidin beads and analyzed by mass spectrometry. As a control, cells without the APEX fusion protein will be treated with the same substrate and catalyst to provide a baseline level of endogenous biotinylation.

Establishing a method to IP ZFHX4 is necessary to ask the following questions about ZHFX4 activity. This approach will reveal whether CHD4, or other NuRD subunits, physically interacts with the TF ZFHX4 during human corticogenesis. Such an interaction would support the hypothesis that ZFHX4 directs corticogenesis by targeting this chromatin remodeling complex to specific loci rather than directly promoting transcriptional trans-activation.

Next, disrupting ZFHX4 binding to CHD4 will allow us to assess the role of their interaction in corticogenesis. Generating structural deletions of ZFHX4 domains, followed by co-IP of exogenously expressed ZFHX4 and CHD4 in phNPCs, will systematically test whether they mediate the interaction between these two proteins. If these domains do not appear to be responsible for the interaction, systematic deletions of ZFHX4 can be conducted instead to perform co-IP. After identifying the domain(s) that are needed for interaction with CHD4, conduct rescue experiments can be conducted in ZFHX4-knockout phNPCs by expressing wildtype or ZFHX4 interaction-deficient mutants in differentiated phNPCs and assess for changes in neural progenitor behavior using ICC, as previously outlined. These experiments will reveal whether interaction with the NuRD complex is critical for ZFHX4 regulation of corticogenesis, and the extent to which ZFHX4 activity is facilitated by the NuRD complex.

However, if this interaction fails to be observed in phNPCs, an unbiased approach can be taken to define its downstream mechanism using proteomic Co-IP datasets to identify candidate interactors to study. Next, ChIP-seq of ZFHX4 in phNPCs to identify the genomic targets of ZFHX4 can be performed. Lastly, performing ATAC-seq in phNPC cultures where ZFHX4 has been knocked out will allow us to map changes in chromatin architecture mediated by ZFHX4. Integrating the ZFHX4 binding profile, and the dysregulation in chromatin accessibility and gene expression caused by its loss, will provide a robust picture of its primary and secondary regulatory programs.

As outlined, this experimental plan will allow the functionally interrogation of the role of the candidate TF ZFHX4 in cortical neurogenesis. By leveraging CRISPR-based genome editing, scRNA-seq technology, and unbiased biochemical approaches to elucidate the molecular mechanisms of neurogenesis, these studies are expected to provide novel biological insights into mechanisms of human cortical expansion and neuropsychiatric disease.

References

Butler, A., Hoffman, P., Smibert, P., Papalexi, E., & Satija, R. (2018). Integrating single-cell transcriptomic data across different conditions, technologies, and species. *Nature Biotechnology*, *36*(5), 411–420. https://doi.org/10.1038/nbt.4096

Chen, C.-L., & Perrimon, N. (2017). Proximity-dependent labeling methods for proteomic profiling in living cells. *Wiley Interdisciplinary Reviews. Developmental Biology*, *6*(4). https://doi.org/10.1002/wdev.272

Chudnovsky, Y., Kim, D., Zheng, S., Whyte, W. A., Bansal, M., Bray, M.-A., Gopal, S., Theisen, M. A., Bilodeau, S., Thiru, P., Muffat, J., Yilmaz, O. H., Mitalipova, M., Woolard, K., Lee, J., Nishimura, R., Sakata, N., Fine, H. A., Carpenter, A. E., … Chheda, M. G. (2014). ZFHX4 interacts with the NuRD core member CHD4 and regulates the glioblastoma tumor initiating cell state. *Cell Reports*, *6*(2), 313–324. https://doi.org/10.1016/j.celrep.2013.12.032

de la Torre-Ubieta, L., & Bonni, A. (2008). Combinatorial assembly of neurons: From chromatin to dendrites. *Trends in Cell Biology*, *18*(2), 48–51. https://doi.org/10.1016/j.tcb.2007.12.003

de la Torre-Ubieta, L., Stein, J. L., Won, H., Opland, C. K., Liang, D., Lu, D., & Geschwind, D. H. (2018). The Dynamic Landscape of Open Chromatin during Human Cortical Neurogenesis. *Cell*, *172*(1–2), 289-304.e18. https://doi.org/10.1016/j.cell.2017.12.014

Heinz, S., Benner, C., Spann, N., Bertolino, E., Lin, Y. C., Laslo, P., Cheng, J. X., Murre, C., Singh, H., & Glass, C. K. (2010). Simple Combinations of Lineage-Determining Transcription Factors Prime cisRegulatory Elements Required for Macrophage and B Cell Identities. *Molecular Cell*, *38*, 576–589.

Hoffmann, A., & Spengler, D. (2019). Chromatin Remodeling Complex NuRD in Neurodevelopment and Neurodevelopmental Disorders. *Frontiers in Genetics*, *10*, 682. https://doi.org/10.3389/fgene.2019.00682

Macosko, E. Z., Basu, A., Satija, R., Nemesh, J., Shekhar, K., Goldman, M., Tirosh, I., Bialas, A. R., Kamitaki, N., Martersteck, E. M., Trombetta, J. J., Weitz, D. A., Sanes, J. R., Shalek, A. K., Regev, A., & McCarroll, S. A. (2015). Highly parallel genome-wide expression profiling of individual cells using nanoliter droplets. *Cell*, *161*(5), 1202–1214. https://doi.org/10.1016/j.cell.2015.05.002

Mellacheruvu, D., Wright, Z., Couzens, A. L., Lambert, J. P., St-Denis, N. A., Li, T., Miteva, Y. V., Hauri, S., Sardiu, M. E., & Low, T. Y. (2013). The CRAPome: A contaminant repository for affinity purificationmass spectrometry data. *Nature Methods*, *10*, 730–736.

Polioudakis, D., de la Torre-Ubieta, L., Langerman, J., Elkins, A. G., Shi, X., Stein, J. L., Vuong, C. K., Nichterwitz, S., Gevorgian, M., Opland, C. K., Lu, D., Connell, W., Ruzzo, E. K., Lowe, J. K., Hadzic, T., Hinz, F. I., Sabri, S., Lowry, W. E., Gerstein, M. B., … Geschwind, D. H. (2019). A Single-Cell Transcriptomic Atlas of Human Neocortical Development during Mid-gestation. *Neuron*, *103*(5), 785-801.e8. https://doi.org/10.1016/j.neuron.2019.06.011

Ronan, J. L., Wu, W., & Crabtree, G. R. (2013). From neural development to cognition: Unexpected roles for chromatin. *Nature Reviews Genetics*, *14*(5), 347–359. https://doi.org/10.1038/nrg3413

Sokpor, G., Xie, Y., Rosenbusch, J., & Tuoc, T. (2017). Chromatin Remodeling BAF (SWI/SNF) Complexes in Neural Development and Disorders. *Frontiers in Molecular Neuroscience*, *10*. https://doi.org/10.3389/fnmol.2017.00243

Stein, J. L. & de la Torre-Ubieta. (2014). A Quantitative Framework to Evaluate Modeling of Cortical Development by Neural Stem Cells. *Neuron*, *83*, 69–86.

Stein, J. L., de la Torre-Ubieta, L., Tian, Y., Parikshak, N. N., Hernández, I. A., Marchetto, M. C., Baker, D. K., Lu, D., Hinman, C. R., Lowe, J. K., Wexler, E. M., Muotri, A. R., Gage, F. H., Kosik, K. S., & Geschwind, D. H. (2014). A Quantitative Framework to Evaluate Modeling of Cortical Development by Neural Stem Cells. *Neuron*, *83*(1), 69–86. https://doi.org/10.1016/j.neuron.2014.05.035

Sweeney, L. B., Bikoff, J. B., Gabitto, M. I., Brenner-Morton, S., Baek, M., Yang, J. H., Tabak, E. G., Dasen, J. S., Kintner, C. R., & Jessell, T. M. (2018). Origin and Segmental Diversity of Spinal Inhibitory Interneurons. *Neuron*, *97*(2), 341-355.e3. https://doi.org/10.1016/j.neuron.2017.12.029

Taupin, P. (2007). BrdU immunohistochemistry for studying adult neurogenesis: Paradigms, pitfalls, limitations, and validation. *Brain Research Reviews*, *53*(1), 198–214. https://doi.org/10.1016/j.brainresrev.2006.08.002

Ward, L. D., & Kellis, M. (2012). Interpreting noncoding genetic variation in complex traits and human disease. *Nature Biotechnology*, *30*(11), 1095–1106. https://doi.org/10.1038/nbt.2422